Cellular and Molecular Life Sciences (2025) 82:387
https://doi.org/10.1007/s00018-025-05890-8

ORIGINAL ARTICLE

Intersectin1/cdc42 signaling regulates methamphetamine-induced neuronal remodeling in the hippocampus

Ana Filipa Terceiro[1,2,3] · Andrea Lobo[1] · Renato Socodato[1,2] · Teresa Canedo[1,4,5] · Ana Isabel Silva[1,2] · Bruno Cavadas[1] · Lia G. Carvalhais[1,6] · Miguel Aroso[1] · Gabriela M. Morello[1] · Paulo Aguiar[1] · Ana Magalhães[1,2,3] · Ana Luísa Carvalho[7,8,9] · João B. Relvas[1,2,10] · Rosalina Fonseca[1,2] · Teresa Summavielle[1,2,11]

Received: 7 February 2025 / Revised: 31 July 2025 / Accepted: 25 August 2025

Abstract

The development and maintenance of drug addiction triggered by psychoactive substances, such as methamphetamine (Meth), is strongly influenced by synaptic and morphological adaptations in the brain. The hippocampus has a key role in the formation of maladaptive drug-context associations and relapse. However, the mechanisms regulating this complex process are not completely understood. Recent studies highlight that the actin cytoskeleton and its regulatory proteins play a fundamental role in morphological and behavioral plasticity associated with drug use. Here, we show that a binge pattern of Meth administration is sufficient to increase hippocampal neurite outgrowth and dendritic spine density leading to augmented basal synaptic transmission and impaired long-term potentiation (LTP) response. To study the molecular pathways affected by Meth, we used embryonic primary neuron cultures from the hippocampus and performed RNA Sequencing from isolated soma or neurites compartments, FRET microscopy, biochemical analyses, and morphometric measurements of dendrites to demonstrate that intersectin (Itsn)1/cdc42 signaling is an important mediator of Meth-induced morphological adaptations, specifically in the synaptic compartment. Furthermore, AAV-mediated depletion of neuronal cdc42 in the hippocampus prevented Meth-induced changes in cytoarchitecture and their consequent impact on neuronal functionality. Our results highlight relevant compartment-associated changes in the activity of Itsn1/cdc42 pathway that critically regulate Meth-induced neuronal remodeling and plasticity.

Keywords rhoGTPases · Addiction · Psychostimulants · Neuronal-morphology · Synaptic plasticity

Ana Filipa Terceiro and Andrea Lobo contributed equally to this work.

✉ Teresa Summavielle
tsummavi@i3s.up.pt

[1] i3S – Instituto de Investigação e Inovação em Saúde, Universidade do Porto, Porto, Portugal

[2] IBMC – Instituto de Biologia Molecular e Celular, Universidade do Porto, Porto, Portugal

[3] ICBAS – Instituto de Ciências Biomédicas Abel Salazar, Universidade do Porto, Porto, Portugal

[4] School of Medicine, Life and Health Sciences Research Institute (ICVS), University of Minho, Braga, Portugal

[5] ICVS/3B's – PT Government Associate Laboratory, Braga, Guimarães, Portugal

[6] Donders Institute for Brain Cognition and Behaviour, Radboud University, 6525 AJ Nijmegen, The Netherlands

[7] CNC- Centre for Neuroscience and Cell Biology, University of Coimbra, Coimbra, Portugal

[8] CiBB- Center for Innovative Biomedicine and Biotechnology, University of Coimbra, Coimbra, Portugal

[9] Department of Life Sciences, Faculty of Sciences and Technology, University of Coimbra, Coimbra, Portugal

[10] Departamento de Biomedicina da Faculdade de Medicina da Universidade do Porto (FMUP), Porto, Portugal

[11] School of Health, Polytechnic Institute of Porto, Porto, Portugal

Published online: 06 November 2025

Introduction

Addiction is a chronic disorder characterized by a compulsive consumption of psychoactive substances despite adverse consequences. The relapsing nature of this disorder is, in part, attributable to drug-induced alterations to the systems regulating cognition, motivation and emotion [1].

Exposure to psychoactive substances, such as methamphetamine (Meth), can disrupt hippocampal function, hampering the acquisition of adaptive behavior that could support drug cessation [2]. North and colleagues [3] demonstrated that following 14 days of Meth administration, mice displayed deficits in spatial memory during the drug abstinence period. Likewise, repeated Meth administration (10 mg/kg, twice daily, for 5 days) also reduced LTP in ex-vivo hippocampal slice preparations and affected excitatory synaptic transmission [4]. Importantly, memory impairments have also been observed several days after exposure to a binge administration of Meth in rats [5–7], indicating that acute exposure to Meth is sufficient to cause persistent hippocampal dysfunction.

Meth can induce long-term modification of neuronal arborization and dendritic spines in the brain reward system [8–11]. This requires reorganization of the actin cytoskeleton that is carried out by Rho GTPases, well-known regulators of the actin cytoskeleton, cell motility and polarity, axon guidance and vesicle trafficking [12]. The spatial activity of these proteins, which cycle between active GTP-bound and inactive GDP-bound conformations, is tightly regulated by GEFs (guanine exchange factors), GAPs (GTPase-activating proteins) and GDIs (guanine nucleotide-dissociation inhibitors) [12–15]. Several studies have indicated that the Rho GTPases rac1 and cdc42 play a significant role in modulating psychostimulant-induced plasticity and subsequently, drug-seeking and taking behaviors [9–11].

Ding and colleagues have shown that a low dose of Meth (2 mg/kg, 4 times, every other day) activates cdc42 and leads to an increase in dendritic spine density, improving spatial memory [11]. In addition, repeated cocaine exposure has been shown to activate cdc42 in the hippocampus, resulting in increased dendritic spine density [16]. However, the upstream regulatory mechanisms leading to cdc42 activation and the role of cdc42 in the regulation of synaptic plasticity after Meth administration remain unclear.

Cdc42 is important for maintenance of dendritic spine density, memory recall [17] and its activity seems to be restricted to stimulated spines [18, 19]. Among cdc42 regulators, Intersectin1 (Itsn1), a scaffold protein, was shown to regulate dendritic spine development and maturation and LTP [20–22]. Double knockout of Itsn1 and its homolog Itsn2, leads to morphological and electrophysiological defects in the cortico-striatal circuitry [23]. We have recently demonstrated that modulation of cdc42 efficiently prevents Meth-induced release of glutamate in astrocytes [24].

Here, based on an RNA Sequencing (RNASeq) analysis of isolated neurites of primary hippocampal neurons, we investigated if Meth-induced cdc42 activation could be regulated through its activator Itsn1. We show that an acute, binge pattern of Meth administration [25] is sufficient to induce hippocampal neurite outgrowth and increase dendritic spine density and maturation, altering basal synaptic connectivity and plasticity. We showed activation of cdc42 in the hippocampal synaptic fraction of WT mice exposed to binge Meth, and that AAV-mediated neuronal cdc42 depletion in the hippocampus prevented Meth-induced increase in neurite arborization, dendritic spine density and functional plasticity response. Our findings confirm that excitatory signaling is dysregulated upon Meth administration and that the Itsn1/cdc42 signaling is a key regulator of neuronal response in the hippocampus, in a synapse-specific manner.

Material and methods

Animals

All mice experiments were conducted following the Directive 2010/63/EU, Portuguese law (DL 113/2013), and approved by Direcção Geral de Alimentação e Veterinária (DGAV) and i3S Animal Ethical Committee (DGAV ref.003891/2019–02-15 and ref.2018–13-TS, respectively). Researchers involved in animal experimentation were FELASA certified. All efforts were made to minimize animal suffering and the number of animals used. Mice were housed under specific pathogen-free conditions, controlled environment (20 °C, 45–55% humidity) with an inverted 12 h/12 h light/dark cycle, and free access to food and water. C57BL/6 and $cdc42^{fl/fl}$ male mice were obtained from the i3S animal facility. Mice homozygous for the cdc42 floxed allele ($cdc42^{fl/fl}$) were backcrossed at least for 10 generations and kept in C57BL/6 background at the i3S animal facility. Genotype was determined by PCR on genomic DNA. Primers for cdc42 floxed alleles were: forward (MR6): 5'TCTGCCATCTACACATACAC3' and reverse (MR7): 5'ATGTAGTGTCTGTCCATTGG3'.

In vivo neuronal labeling

To achieve sparse labeling of neurons in the CNS, AAV (PHP.eB)-CAG-GFP (Addgene, 37825-PHPeB) or (PHP.eB)-CAG-tdTomato (Addgene, 59462-PHPeB) in a final titer of 0.5×10^{11} viral particles diluted in sterile PBS, were injected into the tail vain of adult male C57BL/6 or $cdc42^{fl/fl}$ respectively.

In vivo cdc42 silencing

One week following intravenous AAV injection, $cdc42^{fl/fl}$ mice were injected with pENN.AAV.hSyn.HI.eGFP-Cre.WPRE.SV40 (Addgene, 105540-AAV9), to achieve cdc42 deletion or pAAV-hSyn-EGFP (Addgene, 50465-AAV9) into the hippocampus, in a final titer of 1.2×10^{10} viral particles *per* hippocampus, diluted in sterile PBS. For this, animals were anesthetized with isoflurane and placed on a digitally controlled stereotaxic apparatus equipped with an integrated microinjection system (Stoelting Co.). Rectal temperature was maintained at 37.2 ºC throughout the surgical procedure, using a rectal probe (Stoelting Co.). The mice's fur was shaved and disinfected before making a small incision to expose the cranium. A small hole was drilled in the cranium to allow AAVs injection using the following coordinates (AP) -2.0 mm; (ML) ± 1.3 mm from the bregma; (DV) -2.2 mm from the brain surface, injecting 1 µl per hippocampus at a rate of 0.2 µl/min.

Meth administration in mice

Four to five weeks after intravenous AAVs injection for neuronal labeling, mice received either 4 × 5 mg/kg Meth, with 2 h intervals between injections, intraperitoneally (i.p.) or 4 × isovolumetric saline injections, as previously described [26]. Meth hydrochloride was acquired from Sigma Aldrich under Infarmed license (ref. 290–13).

Hippocampal slice preparation for electrophysiological recordings

Twenty-four hours after the first Meth or saline administration, mice were euthanized by cervical dislocation. The brains were quickly removed and immersed in ice-cold artificial cutting cerebro-spinal fluid (ACSF) for sectioning. All experiments were performed in transverse hippocampal slices. Cutting ACSF was saturated with 95%O_2/5%CO_2 and contained (in mM): NaCl 126, KCl 2.5, NaH_2PO_4 1.25, $NaHCO_3$ 26, $MgCl_2$ 5, $CaCl_2$ 1, Glucose 25. The hippocampi were isolated and cut into 400 µm-thick transverse slices using a tissue slicer (Siskiyou, Inc.). Slices were maintained in ACSF at 32º C for at least one hour before recording. They were then transferred to a submersion chamber and continuously perfused (1.5–2 ml/min) with recording ACSF at 32º C. The recording ACSF was saturated with 95%O_2/5%CO_2 and contained (in mM): NaCl 126, KCl 2.5, NaH_2PO_4 1.25, $NaHCO_3$ 26, $MgCl_2$ 2, $CaCl_2$ 2.8, Glucose 25.

Electrophysiological recordings

Recordings started after 20 min of resting in the recording chamber. Schaffer collaterals were stimulated with 0.2 ms pulses using monopolar epoxy-insulated tungsten electrodes (Science Products, GmbH, Germany). Field excitatory postsynaptic potentials (fEPSP) were recorded extracellularly in the stratum radiatum of the CA1 region (~130 µm below the slice surface) using glass microelectrodes filled with 3 M NaCl (immobilized with agarose—tip resistance 3-5MOhm). Stimulus intensities were set to evoke 50% of the maximal fEPSP slope. The test pulse frequency was 0.33 Hz. Synaptic plasticity was induced after recording a stable 15 min baseline of fEPSPs.

Induction of synaptic plasticity

After baseline stimulation, one of the pathways was arbitrarily chosen to induce LTP. This input received a tetanus of 25 pulses at a frequency of 100 Hz, repeated 5 times with a 3 s interval. The second input served as a control pathway and was continuously recorded. For long-term depression (LTD) induction, one of the pathways was stimulated with a low frequency burst stimulation (LFS—3 pulses per burst at 20 Hz, 900 bursts repeated at 1 Hz). Analysis of input/output responses was done by averaging three consecutive synaptic responses evoked by increasing input injected current, based on the maximum fEPSP response (100%, 75%, 50% and 25% of maximum fEPSP response). Data points correspond to the average of three consecutive pulses for each value of injected current and averaged crossed experiments.

Electrophysiological data analysis

Electrophysiological data were collected using a Dagan IX2-700 amplifier (Dagan Corporation, Minnesota, USA) and band-pass filtered (low pass 1 kHz, high pass filter 1 Hz, LHBF 48X, NPI Electronic GmbH, Germany). Data were sampled at 5 kHz using a Lab-PCI-6014 data acquisition board (National Instruments, Austin, TX) and stored on a PC. Offline data analysis was performed using a customized LabView-program (National Instruments). As a measure of synaptic strength, the initial slope of the evoked fEPSPs was calculated and expressed as percent changes from the baseline mean. Error bars denote SEM values. Experiments were excluded if the control pathways decayed more than 20% below baseline. For the LTP analysis, LTP values were averaged in 5 min data bins at two-time windows—initial

5 min after LTP induction (T1 = 15 to 20 min) and at the end of the recorded time (T2 = 70 to 75 min). The percentage of LTP decay was calculated by [(T1-T2)/T1*100]. For LTD analysis, LTD values were also averaged in 5 min data bins at two-time windows – initial 5 min after LTD induction (T1 = 15 to 20 min) and at the end of the recorded time (T2 = 70 to 75 min). These were then compared across time and conditions.

Pull-down assay for active cdc42 and Itsn1/cdc42 pathway in synaptoneurosome

To perform a pull-down assay for active cdc42, mice were euthanized by cervical displacement 15 min after the last Meth or saline administration of the binge protocol- The hippocampi were quickly dissected on ice and synaptosomes were isolated using the Syn-PER Synaptic Protein Extraction Reagent (87793, ThermoFisher Scientific) according to the manufacturer's instructions. Cdc42 activity was measured using the Pull-down Activation Assay Biochem Kit (#BK034, Cytoskeleton), according to the manufacturer's instructions. For western blot analysis of Itsn1/cdc42 pathway, following protein extraction, samples were denatured with 4 × concentrated denaturating buffer (277.8 mM Tris (pH 6.8), 4.4% SDS, 40% glycerol, 10% β-mercaptoethanol, and 0.1% bromophenol blue) and boiled to 60 °C for 10 min. Protein samples were separated by SDS-PAGE, in 7.5% or 10% polyacrylamide gels, transferred to nitrocellulose membranes (Bio-Rad), and unspecific binding was blocked by incubating with 5% skim milk in Tris-buffered saline solution with 0.1% Tween 20 (TBS-T). Membranes were incubated with primary antibodies overnight at 4 °C under constant rotation, washed, and exposed to horseradish peroxidase-conjugated secondary antibodies anti-mouse (1:3000, 31432 Thermo Scientific Pierce) and anti-rabbit (1:10 000, A0545 Sigma Aldrich) for 1 h at room temperature. Horseradish peroxidase activity was visualized by chemiluminescence (ECL) on the ChemiDoc system (BioRad) and quantified using the ImageLab software v6.0.1 (BioRad). The primary antibodies used were anti-Itsn1 (1:1000, 611574, BD Biosciences), anti-N-WASP (1:1000, WP2001, ECM Biosciences), anti-pN-WASP(Tyr256) (1:1000, WP2601, ECM Biosciences), anti-Arp3 (1:1000, AP4581, ECM Biosciences) and anti-GAPDH (1:5000, 5G4, HyTest).

Neuronal morphometric analysis

Animals were anesthetized and perfused with ice-cold PBS, followed by 4% PFA. Brains were post-fixed overnight, cryoprotected in 30% sucrose and embedded in OCT, frozen and cryosection coronally at 60–80 µm in the CM30550S cryostat (Leica Biosystems). Brain sections were then incubated (free floating) with blocking solution (10% horse serum, 0.2% Triton X-100 in PBS) for 1 h at RT. Then, slices were incubated with primary antibodies anti-GFP (1:500, Roche) and anti-tdTomato (1:500, HBT020-200, HenBiotech), in blocking solution for 72 h at 4ºC under agitation. Afterward, slices were washed with PBS and incubated with the secondary antibodies anti-mouse A488 (1:500, A11001, Invitrogen) and anti-goat A647 (1:500, ab98157, abcam) for 24 h at 4ºC and nuclei stained with DAPI. Lastly, sections were mounted in gelatin-coated slides using DAKO mounting medium, sealed with nail polish and stored at 4ºC protected from light.

Images of neurons in the CA1 region of the hippocampus were acquired in a Leica TCS SP5II confocal microscope (Leica microsystems, Germany), with a 40X/1.1 NA water objective, 1024 × 1024 resolution, at a step-size of 0.17 µm. Neurons expressing GFP (in C57BL/6 mice) or GFP and tdTomato (in $cdc42^{fl/fl}$) were randomly selected for quantification. Neuron tracing was performed using NeuronJ plugin for ImageJ software and Sholl analysis as previously described using Bonfire scripts for MATLAB [27]. For dendritic spine density and morphology analysis, images from secondary dendrites of hippocampal CA1 neurons expressing GFP (in C57BL/6 mice) or GFP and tdTomato (in $cdc42^{fl/fl}$) were acquired with a 63x/1.3 NA glycerol objective, at 6.28 × zoom, 1024 × 1024 resolution and 0.08 µm step-size. Acquired images were deconvoluted using Huygens Professional 20.04. Spine morphology was defined as filopodia (without a defined head), thin (with a long neck and a small head), mushroom (with a small neck and a large head) and stubby (without a defined neck) using ImageJ software, as before [27]. The number of dendritic spines was represented *per* 10 µm of dendritic length.

Hippocampal neuronal cultures

Primary hippocampal neuronal cultures were prepared from E16 C56BL/6 mice embryos as previously described [27]. Briefly, the dissected hippocampi were treated with trypsin (0.06%, 10 min, 37ºC) (Gibco, ThermoFisher Scientific) in Hank's salt solution (HBSS) (Gibco, ThermoFisher Scientific). The tissue was dissociated in serum-free Neurobasal medium (Gibco, ThermoFisher Scientific), supplemented with B27 (Gibco, ThermoFisher Scientific), glutamate (25 µM) (Sigma Aldrich), glutamine (0.5 mM) (Sigma Aldrich) and gentamicin (0.12 mg/mL) (Gibco, ThermoFisher Scientific). Neurons were plated on poly-d-lysine (PDL) coated cell culture plates at 8×10^4 cells/cm^2 in coverslips for transfection and 8.8×10^4/cm^2 in 3 µM pore size Boyden chambers (#353,091, Corning Life Sciences)

for RNA extraction. Cells were kept at 37ºC in a humified incubator with 5% CO_2/ 95% O_2 for 14DIV. For synaptic proteins analysis, neurons were plated on PDL-coated coverslips at a density of 2.5×10^3 cells/cm^2, with surrounding cortical neurons for trophic support, as previously described [28]. Cells were kept at 37 °C in a humidified incubator with 5% CO_2/95% air and treated at 20DIV with PBS (Control) or 100 µM Meth for 24 h.

RNA extraction

At 14DIV, neurons cultured in Boyden chambers were exposed to PBS (Control) or 100 µM Meth for 24 h. Afterwards, total RNA was extracted using TRIzol (Ambion, Life Technologies) and Quick-RNA MicroPrep (Zymo Research), according to the manufacturer's instructions. For compartmentalized analysis, the upper Boyden chamber was scraped with a TRIzol impregnated swab and emerged in TRIzol to extract soma fractions, while Boyden chambers were submerged in TRIzol and scraped to extract RNA from neurite fraction. cDNA synthesis was conducted using RT^2 HT First Strand kit (Qiagen), following manufacturer's instructions and stored at -80ºC until further use.

RNA Seq analysis

Sequence alignment was carried in STAR v2.7.10a with the mouse GRCm39 reference (GENCODE vM33). Counts per gene were generated by STAR. Prior to alignment, reads were pre-processed in TrimGalore to remove adapters sequences. If after adapter trimming the resulting read had a length below 35 bp, it was removed from the analysis. Differential expression (DE) analysis was carried in R v4.1.2 using DESeq2 (v1.34). Gene-set enrichment analysis, using the pre-ranked list of genes (signed log2FC x -log10(padj)) was carried in fgsea. Only pathways with and FDR below 0.25 were considered. STRING database (version 12.0) was used to find the first shell (first 10) of interactors of genes of interest.

Transfection and cell treatments

Cultured hippocampal neurons were transfected at 11DIV using the calcium phosphate precipitation method, as previously described [27], with 2 µg of plasmid DNA per coverslip, using myrGFP (pCAGGS-myrGFP was kindly offered by Thomas Biederer (Addgene plasmid #115,502) [29]), dominant negative form of cdc42 (cdc42 DN) or a microRNA to target Itsn1 (miRNA Itsn1), kindly offered by Peter S McPherson [20], that targets Intersectin1 mRNA at nucleotide 2085 and expresses EmGFP as a reporter. Two-to-three days after transfection, neurons were treated with PBS (Control) or 100 µM Meth for 24 h.

Immunocytochemistry and image analysis

After treatment, cells were fixed in 4% PFA in PBS containing 4% sucrose for 10 min at room temperature (RT), permeabilized with 0.3% Triton X-100 and blocked with 5% BSA for 1 h at RT. Then, primary antibodies were incubated overnight at 4ºC, washed and incubated with the secondary antibodies for 1 h at RT. After washing, cells were stained with Hoechst 33,342 (0.5 µg/ml) for 10 min at RT and coverslips were mounted with DAKO mounting media, sealed with nail polish and stored at 4ºC in the dark. Primary antibodies used were GFP (1:500, 11814460001, Roche, Sigma), PSD95 (1:500, MA1-045, Invitrogen) and VGLUT1 (1:1000, 135 308, Synaptic systems); secondary antibodies were anti-mouse A488 (1:500, A11001, Invitrogen) and anti-rabbit 594 (1:500, A11012, Invitrogen).

Slides were imaged using the Leica TCS SP5II confocal microscope (Leica microsystems, Germany), with a 40x/1.1 NA water objective. Neuronal morphology, ramification and dendritic spine morphology and density were analyzed as described above (see neuronal morphometric analysis). For synaptic protein colocalization, images were analyzed using ImageJ, as described elsewhere [30]. Briefly, isolated segments of neurites containing both PSD95 and VGLUT1 staining were selected and thresholded to select recognizable puncta and measured for number, area and intensity, per dendritic length. The background value was subtracted from the obtained intensity value, and this result was multiplied by the puncta area, obtaining the intensity per area. The thresholded VGLUT channel was set as binary and PSD95 channel was used to define the total puncta. The puncta positive for VGLUT1 and PSD95 were defined as colocalized.

FRET assays

Cultured hippocampal neurons were transfected at 11DIV using the calcium phosphate method, as above, with the FRET reporter RaichuEV-cdc42, provided by M. Matsuda [31]. Two-days after transfection, neurons were treated with 100 µM Meth for 5, 10, 15 and 30 min, or PBS, and fixed in 4% PFA in PBS containing 4% sucrose for 10 min at RT. Images of dendritic segments with distinguishable dendritic spines were acquired in a Leica TCS SP8 microscope using a 63x/1.3 NA glycerol objective. FRET/Donor ratio at dendritic spines was calculated for each time point and normalized for PBS-exposed neurons.

Statistical analysis

All experimental conditions were compared to their respective controls. The experimental unit considered (animal,

slice, culture, cell or dendrite segment) and statistical test used is detailed in the corresponding figure legends. Graphical representations and removal of outliers (using the ROUT method with Q = 1%) were conducted in GraphPad Prism (version 10.0.2).

Data is presented as mean ± standard error of the mean (SEM). Statistical analysis was performed using GraphPad Prism or SAS Visual Statistics using a linear mixed model, followed by Tukey–Kramer multiple comparison test, using the culture or the animal as a random variable (for experiments conducted in cultured primary hippocampal neurons and for experiments conducted in animals, respectively). All data was assessed for residuals' normality through the quantile–quantile plot, and non-normally distributed data was transformed (using square root, cube root or log10 functions). Significance was set at $p < 0.05$. Figure panels were created using Adobe Illustrator 2021 (version 25.1) and schematic representations were created using BioRender.

Results

Meth drives structural remodeling, disrupting synaptic plasticity in the hippocampus

To investigate the impact of Meth on hippocampal structure and function, we employed a well-established binge administration model (4 × 5 mg/kg of Meth, every 2 h), mimicking patterns of Meth use in humans [32]. Neuronal morphology at the CA1 region of the hippocampus was analyzed using GFP reporter AAV particles intravenously injected in adult mice [27], a highly efficient method for sparse labeling of CNS neurons. This approach allowed precise tracking of Meth-induced structural remodeling at the single-cell level. Tissues were harvested 24 h after the first Meth dose to capture early neuronal adaptations to drug exposure (Fig. 1A and B).

Meth exposure led to a marked increase in total neurite length (Fig. 1C) and a sholl analysis further demonstrated increased dendritic complexity, with a higher number of intersections at increasing distances from the soma (Fig. 1D). Representative neuronal tracings illustrated the extent of these changes, revealing an expanded and more intricate dendritic tree in Meth-treated neurons (Fig. 1E). This suggests that Meth enhances neuronal structural plasticity, potentially altering the balance of excitatory connectivity in hippocampal circuits.

Dendritic spine density, a key determinant of excitatory synaptic connectivity was also significantly affected following Meth exposure. We found that Meth-treated mice displayed an increase in total spine density (Fig. 1F and G), which was found across mushroom (mature, more stable spines) and stubby spines (Fig. 1H and I). On the other hand, Meth administration did not significantly affect the density of thin or filopodia (more dynamic and exploratory

Fig. 1 Meth Drives Structural Remodeling, Disrupting Synaptic Plasticity in the Hippocampus **A**: Schematic representation of experimental timeline. Adult male C57BL/6 mice were intravenously injected with an AAV_PHP.eB for GFP transduction in the CNS. Twenty-eight days later, mice received a binge administration of 5 mg/kg Meth, i.p. four times, with two-hours interval between each injection or saline (control). Twenty-four hours after the first administration, mice were sacrificed and the morphology of neurons in the CA1 region of the hippocampus analyzed. **B**: Representative image of the region analyzed in the hippocampus (scale bar: 100 µm). Neuronal morphology of hippocampal neurons was analyzed 24h following a binge pattern of Meth or Saline administration. Graphs display (mean ± SEM) **C**: total neurite length ***$p < 0.001$ (linear mixed analysis with the animal fitted as a random effect followed by a Tukey–Kramer correction) and **D**: ramification (sholl) analysis ****$p < 0.0001$ (two-way ANOVA revealing significant effects for treatment ($p < 0.0001$) and distance to cell body ($p < 0.0001$), with interaction between factors ($p < 0.0001$)) of neurons of the CA1 region (n = 7–16 neurons/animal from 4–6 mice per group). **E**: Representative tracings of CA1 neurons. **F**: Representative images of dendritic spines (scale bar: 15 µm). Graphs display (mean ± SEM) **G**: total dendritic spine density, **H**: mushroom spine density, **I**: stubby spine density, **J**: thin spine density, **K**: filopodia spine density *$p < 0.05$ **$p < 0.01$ (linear mixed model analysis with the animal fitted as a random effect followed by a Tukey–Kramer correction) (n = 5–7 dendrite segments/animal, from 3 mice per group). Each circle represents each hippocampal neuron/dendrite segment and each color represents each mouse. **L**: Schematic representation of experimental timeline (top) and hippocampal slice with the positioning of stimulating (S) and recording electrodes (bottom). Adult male C57BL/6 mice received a binge administration of 5 mg/kg Meth, i.p. four times, with two-hours interval between each injection or saline (control). Twenty-four hours after the first administration, mice were sacrificed and the hippocampus collected and sliced for electrophysiological recordings. **M**: Graph displays (mean ± SEM) input/output curve plotted by fEPSPs amplitude against the stimulus intensity ***$p < 0.001$ ****$p < 0.0001$. (two-way ANOVA with two-stage step-up method of Benjamini, Krieger and Yekutiel for multiple comparisons) (n = 9–11 slices from 4 mice per group). **N**: Summary plot of normalized fEPSP slope measurements recorded in the CA1 region of the hippocampus (mean ± SEM) of saline (square symbols) or Meth (circle symbols) treated mice after LTP induction with a tetanus high frequency stimulus. Slice viability was assessed by recording a second independent pathway that did not show a significant decrease throughout the recording (diamond symbols). Top: average fEPSPs at baseline (solid line), T1 (dashed line) and T2 (dotted line). Scale bar: 1 mv, 10 ms. **O**: Summary plot showing the percentage of LTP decay for the time window at T1 and T2. *$p < 0.05$ (unpaired t-test) (n = 10–12 slices from 4 mice per group). **P**: Summary plot of normalized fEPSP slope measurements recorded in the CA1 region of the hippocampus (mean ± SEM) of saline (square symbols) or Meth (circle symbols) treated mice after LTD induction with a low frequency burst stimulation. Slice viability was assessed by recording a second independent pathway that did not show a significant decrease throughout the recording (diamond symbols). Top: average fEPSPs at baseline (solid line), T1 (dashed line) and T2 (dotted line). Scale bar: 1 mv, 10 ms. **Q**: Summary plot showing the percentage of LTD decay for the time window at T1 and T2 **$p < 0.01$ ***$p < 0.001$. (two-way ANOVA with two-stage step-up method of Benjamini, Krieger and Yekutiel for multiple comparisons) (n = 9–11 slices from 4 mice per group)

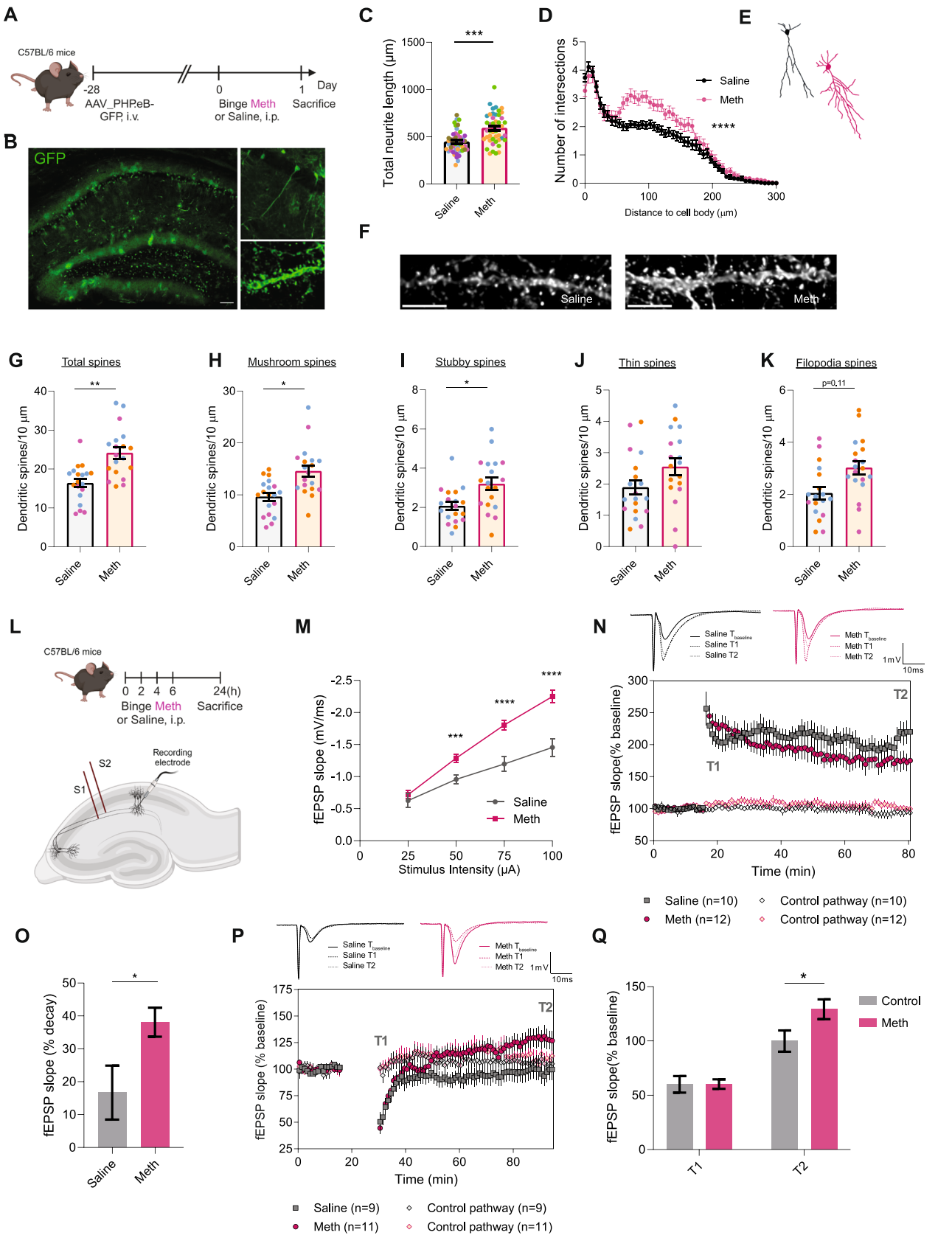
A
C57BL/6 mice
-28
AAV_PHPeB-GFP, i.v.
0
Binge Meth or Saline, i.p.
1
Day
Sacrifice
B
GFP
C
Total neurite length (μm)
***
Saline
Meth
D
Number of intersections
Saline
Meth
****
Distance to cell body (μm)
E
F
Saline
Meth
G
Total spines
Dendritic spines/10 μm
**
H
Mushroom spines
*
I
Stubby spines
*
J
Thin spines
K
Filopodia spines
p=0,11
L
C57BL/6 mice
0 2 4 6
24(h)
Binge Meth or Saline, i.p.
Sacrifice
S1
S2
Recording electrode
M
fEPSP slope (mV/ms)
***
****
****
Saline
Meth
Stimulus Intensity (μA)
N
Saline T baseline
Saline T1
Saline T2
Meth T baseline
Meth T1
Meth T2
1mV
10ms
T1
T2
fEPSP slope(% baseline)
Time (min)
Saline (n=10)
Meth (n=12)
Control pathway (n=10)
Control pathway (n=12)
O
fEPSP slope (% decay)
*
P
Saline (n=9)
Meth (n=11)
Control pathway (n=9)
Control pathway (n=11)
Q
Control
Meth

protrusions) spines (Fig. 1J and K). Furthermore, we examined spine head diameter, a well-established correlate of synaptic strength [33], and found that Meth administration led to a decrease in total and mushroom spine head diameter (Suppl. Figure 1A and B), but did not find differences in thin spine head diameter (Suppl. Figure 1C).

Remodeling of neuronal morphology, and particularly of dendritic spines, is thought to underly the formation and maintenance of memory through enduring alterations in neuronal connectivity [34]. To assess whether these alterations led to an alteration in synaptic content, we stained VGLUT1, a presynaptic marker of glutamatergic terminals and PSD95, a postsynaptic scaffolding marker in hippocampal slices (Suppl. Figure 1D). The colocalization between both markers is thought to correspond to a synapse [35]. Confocal imaging and relative quantification of synaptic puncta in the CA1 region showed that Meth administration did not affect significantly the number of either VGLUT1 structures (Suppl. Figure 1E), PSD95 puncta (Suppl. Figure 1F) or their colocalization (Suppl. Figure 1 G and H).

The presence of both stable and highly dynamic spines raises the question of whether Meth-induced structural plasticity translates into functional improvements or instead disrupts the stability of synaptic transmission. To clarify the effects of Meth on hippocampal function and synaptic plasticity, we recorded synaptic responses in hippocampal slices from adult male mice exposed to binge Meth, 24 h after the first administration (Fig. 1L). We found that in Meth-exposed animals, synaptic responses were significantly higher than in control, suggesting a global increase in synaptic transmission (Fig. 1M). Consistently, we found that systemic exposure to Meth resulted in impaired maintenance of LTP (Fig. 1N). Analysis of LTP decay shows a significantly higher decay in Meth-exposed animals, when compared to controls (Fig. 1O). Interestingly, we found that low-frequency stimulation of Schaffer collateral in control animals induces short-term depression of synaptic responses, followed by a return to the pre-stimulation levels, whereas in Meth-treated animals, the same stimulation led to a transition from short-term depression to LTP (Fig. 1P). The increase in fEPSP slope was significantly higher in Meth-treated versus control mice at T2 (Fig. 1Q), suggesting a disruption in synaptic plasticity induced by binge administration of Meth. Collectively, these results show that a binge administration of Meth leads to significant neuronal remodeling and altered synaptic plasticity in the hippocampus.

Meth also induces neuronal remodeling and affects synaptic activity in primary hippocampal neurons

To determine whether the effects found in hippocampal neurons are cell-autonomous and to explore their underlying mechanisms, we employed primary hippocampal neuron cultures, which are free from systemic influences such as vascular and glial interactions. By isolating the direct effects of Meth on neuronal structure, synaptic organization, and network activity, this approach complements our in vivo observations and provides mechanistic insights into how Meth disrupts synaptic homeostasis.

For this, primary hippocampal neuron cultures were transfected with GFP at 11DIV and subsequently exposed to 100 µM Meth for 24 h at 13DIV [100 µM as in [26, 36]]. Meth-treated neurons increased total neurite length (Fig. 2A and B) and ramification (Fig. 2C), as indicated by Sholl analysis.

Importantly, these alterations were not due to toxicity. Hoechst staining showed no differences in nuclear condensation (Suppl. Figure 2A and B) and MTT assays revealed no significant alterations on mitochondrial function (Suppl. Figure 2C), suggesting that Meth did not promote neurodegeneration.

Furthermore, Meth increased total dendritic spine density (Fig. 2D and E), affecting filopodia (Fig. 2F), thin (Fig. 2G) and mushroom (Fig. 2H) spines, while stubby spine density remained unchanged (Suppl. Figure 2D). To correlate these

Fig. 2 Meth also induces neuronal remodeling and affects synaptic activity in primary hippocampal neurons. **A**: Representative images of primary hippocampal neurons GFP-transfected at 11DIV and treated, at 13DIV, with PBS (Control) or 100 µM Meth for 24h (scale bar: 40 µm). Graphs display (mean ± SEM) **B**: total neurite length ****p < 0.0001 (linear mixed analysis with the culture fitted as random effect followed by a Tukey–Kramer correction) and **C**: ramification (sholl) analysis ****$p < 0.0001$ (two-way ANOVA revealing significant effects for treatment ($p < 0.0001$) and distance to cell body ($p < 0.0001$), with interaction between factors ($p < 0.01$)) (n = 40–55 neurons, from 4–6 independent cultures per group). **D**: Representative images of dendritic spines after PBS (Control) or 100 µM Meth treatment (scale bar: 5 µm). Graphs display (mean ± SEM) **E**: total dendritic spine density, **F**: filopodia spine density, **G**: thin spine density and **H**: mushroom spine density. *$p < 0.05$ **$p < 0.01$ ***$p < 0.001$ (linear mixed analysis with the culture fitted as random effect followed by a Tukey–Kramer correction) (n = 30 dendrite segments from 5 independent cultures). Graphs display summary of cumulative frequency of dendritic spine head diameter of **I**: total spines (n = 1144–1249 dendritic spines from 5 independent cultures), **J**: thin spines (n = 323–374 dendritic spines from 5 independent cultures) and **K**: mushroom spines (n = 462–571 dendritic spines from 5 independent cultures). *$p < 0.05$ ****$p < 0.0001$ (nonparametric Kolmogorov–Smirnov test). **L**: Representative images of low density cultured hippocampal neurons (20DIV) exposed to PBS (Control) or 100 µM Meth for 24h and stained for PSD95 (red) and VGLUT1 (green) (scale bar: 20 µm). Graphs display (mean ± SEM) quantification of **M**: VGLUT1 puncta number, area and fluorescence intensity and **N**: PDS95 puncta number, area and fluorescence intensity, normalized to control levels *$p < 0.05$ (linear mixed analysis with the culture fitted as random effect followed by a Tukey–Kramer correction) (n = 36–38 dendrite segments from 5 independent cultures). Each circle represents a hippocampal neuron/dendrite segment and different colors represent different independent cultures

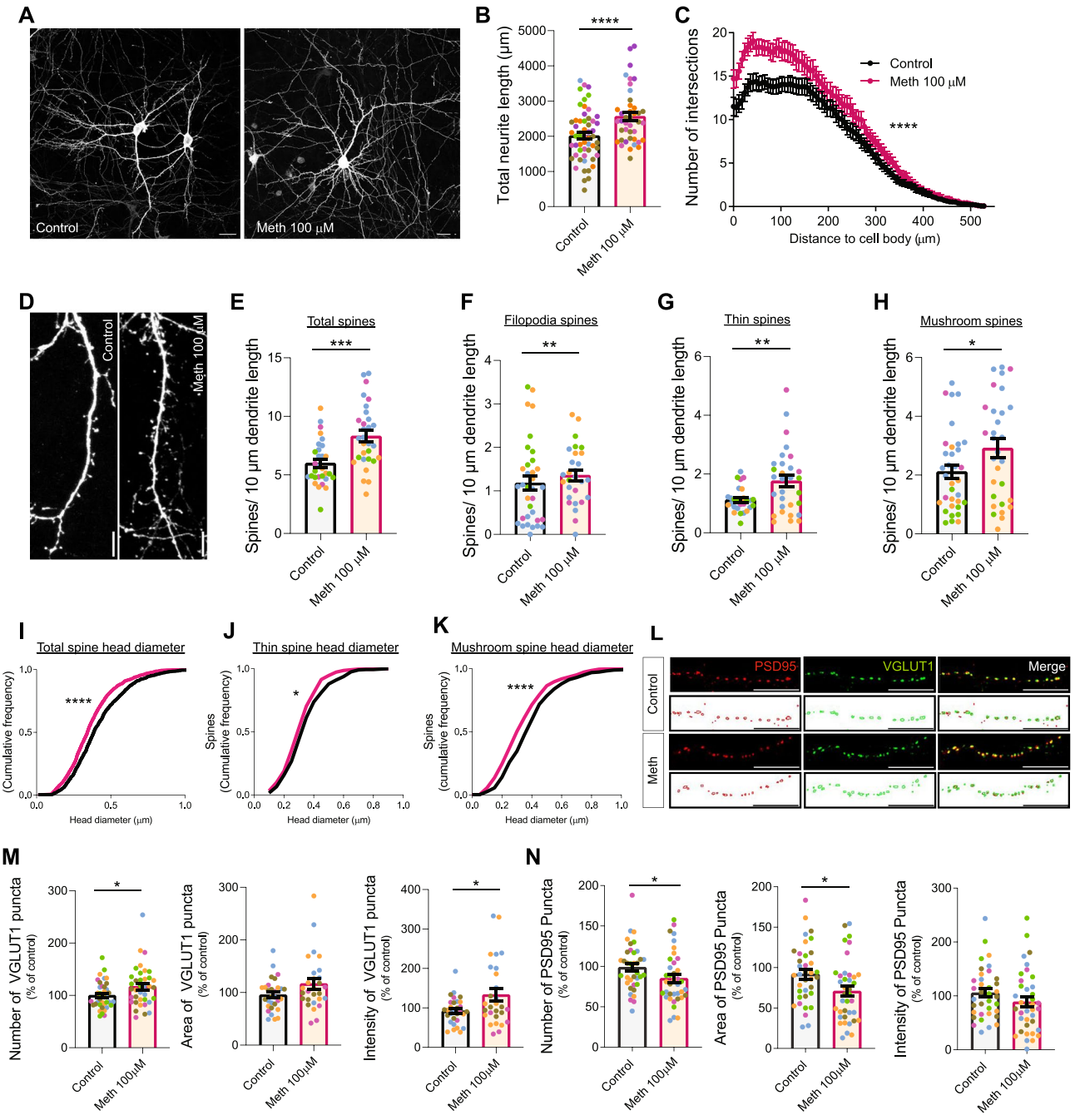

structural changes into functional outcomes, we examined spine head diameter, and found decreased dendritic spine head diameter (Fig. 2I), particularly on thin (Fig. 2J) and mushroom (Fig. 2K) spines. Since larger spine heads correlate with higher AMPA receptors numbers and synaptic stability [37, 38], this reduction suggests that Meth promotes weak and unstable connections.

To assess synaptic content alterations, we evaluated if the number and/or strength of synapses were affected by Meth. For that, we exposed low density cultures of primary hippocampal neurons, which allow the analysis of isolated segments of dendrites, to 100 μM Meth for 24 h and stained these cultures for PSD95 and VGLUT1 (Fig. 2L). Meth increased the number and fluorescence intensity of VGLUT1 puncta indicating an accumulation of presynaptic vesicular content, without affecting their area (Fig. 2M). In contrast, PSD95 puncta number and area were decreased, while its fluorescence intensity remained unchanged (Fig. 2N). The selective loss of PSD95, despite increased dendritic spine density, suggests that Meth weakens postsynaptic stability, potentially impairing receptor anchoring and synaptic maturation [37]. Surprisingly, the number of synapses (PSD95

puncta, colocalized with VGLUT1 puncta) were not altered, neither in number, area nor intensity (Suppl. Figure 2E). This suggests that, despite Meth-induced remodeling of pre- and post-synaptic terminals, these changes do not translate into an increase in functional synapses and reinforces that Meth impairs hippocampal plasticity.

We evaluated the spontaneous neuronal activity of primary cultured hippocampal neurons using microelectrode arrays (MEA; Suppl. Figure 2F). Our findings revealed a significant reduction in neuronal activity six hours after the addition of Meth, followed by a partial recovery at 24 h (Suppl. Figure 2G). This suppression of network activity, despite increased spine density, suggests that Meth disrupts hippocampal function by weakening synaptic strength rather than enhancing excitatory output. The observed decrease in PSD95 expression and spine head diameter, both key determinants of functional synaptic efficacy, likely contribute to the observed loss of spontaneous activity. Thus, rather than enhancing synaptic output, Meth appears to drive a form of maladaptive plasticity. These findings align with our in vivo electrophysiology results, where Meth impaired LTP and LTD while altering basal synaptic transmission.

These results show that, similarly to a binge administration of Meth, primary cultured neurons exposed to 100 µM Meth increase neuronal complexity, dendritic spine density, decrease dendritic spine head diameter, but do not alter the number of synapses. On the other hand, while in vitro Meth-exposure leads to a reduction of neuronal activity, in hippocampal slices of Meth-treated mice, there was an increase in synaptic transmission, but a decrease in LTP. Swant and colleagues (2010) have shown similar results and demonstrated that Meth affects excitatory synaptic transmission via activation of dopamine and serotonin receptors in the hippocampus [4], which could justify the differences observed between hippocampal cultures and slices, since the monoaminergic input is absent in the first.

Overall, we conclude that this model can address signaling pathways regulating Meth-induced neuronal remodeling.

Meth induces spatially restricted dysregulation of Rho GTPase signaling in neurites

Having established that Meth induces significant structural and functional alterations in hippocampal neurons, to investigate the intracellular mechanisms underlying these alterations, primary hippocampal neurons were cultured on a modified Boyden chamber system, to allow for physical separation of the neuronal cell bodies (soma) and neurite fractions (Fig. 3A and B) [39], and exposed to Meth (100 µM) or PBS (Control) for 24 h. RNA from each fraction was collected and RNASeq performed in pooled replicates derived from multiple independent cultures. Samples had comparable sequence counts between them, ranging between 31 and 47 million reads, with a high percentage of mapped reads (between 98.61% and 99.09%), indicating high-quality transcriptomic data.

Gene set enrichment analysis (GSEA) using the gene set derived from the Gene Ontology (GO) molecular function was conducted in the neurite fraction and expressed by the normalized enrichment score (NES) for each ontology term (Fig. 3C). Meth induced an upregulation of ontology terms associated with MAP kinase activity, structural constituents of ribosome and protein tyrosine threonine phosphatase

Fig. 3 Meth Induces Spatially Restricted Dysregulation of Rho GTPase Signaling in Neurites. **A**: Schematic representation of primary hippocampal neurons cultured on a modified Boyden chamber system for 14DIV, to separate soma and neurite fractions for RNA sequencing. **B**: Representative images of upper (soma); lower (neurites) and side compartments of membrane (green: phalloidin, blue: DAPI). **C**: Dot plot of GSEA (molecular function) for neurites in control vs Meth-exposed neurons. **D**: "GTPase cycle" heatmap of the relative expression values (z-score of each gene across sample) found in neurites from control vs Meth-exposed neurons. Each column represents individual experiments, which consist of pools from four independent primary hippocampal neuronal cultures. **E**: Number of repeated interactions established in the first shell of interactors of each term found in neurites involved in "GTPase cycle". **F**: Representative images of primary hippocampal neurons transfected at 11DIV with the Raichu-cdc42 probe and treated, at 13DIV, with PBS (Control) or 100 µM Meth for 5, 10, 15 or 30 min (scale bar: 5 µm). **G**: Graph displays the FRET/Donor ratio in each dendritic spine, normalized to the area of the spine. Symbols represent the mean of each independent cell culture, and the violin plots the variability of all dendritic spines quantified. $^{**}p<0.01$ $^{****}p<0.0001$ (n = 210–248 dendritic spines from 3 independent cultures) (linear mixed analysis with the culture fitted as random effect followed by a Tukey–Kramer correction). **H**: Schematic representation of experimental timeline of hippocampal synaptosome collection. Mice received a binge administration of Meth and were sacrificed 15 min after the last injection. Hippocampal synaptosomes were isolated and a pull-down assay for GTP-bound cdc42 was performed. **I**: Graph displays (mean ± SEM) GTP-bound cdc42/Total cdc42 ratio in synaptosomes of the hippocampus of mice 15 min after treatment with Saline or Meth (4 × 5mg/kg, 2h interval), normalized to control animals $^{*}p<0.05$ (unpaired t-test) (n = 5–6 animals per group). **J**: Graph displays (mean ± SEM) Itsn1/GAPDH ratio in synaptosomes of the hippocampus of mice 15 min after treatment with Saline or Meth (4 × 5mg/kg, 2h interval), normalized to control animals (unpaired t-test revealing no significant differences) (n = 5 animals per group). **K**: Graph displays (mean ± SEM) N-WASP/GAPDH ratio in synaptosomes of the hippocampus of mice 15 min after treatment with Saline or Meth (4 × 5mg/kg, 2h interval), normalized to control animals (unpaired t-test revealing no significant differences) (n = 5 animals per group). **L**: Graph displays (mean ± SEM) pN-WASP/N-WASP ratio in synaptosomes of the hippocampus of mice 15 min after treatment with Saline or Meth (4 × 5mg/kg, 2h interval), normalized to control animals $^{**}p<0.01$ (unpaired t-test) (n = 4–5 animals per group). **M**: Graph displays (mean ± SEM) Arp3/GAPDH ratio in synaptosomes of the hippocampus of mice 15 min after treatment with Saline or Meth (4 × 5mg/kg, 2h interval), normalized to control animals $^{**}p<0.01$ (unpaired t-test) (n = 5 animals per group). **N**: Itsn1 interacts with cdc42 and N-WASP, which leads to actin polymerization via Arp2/3 complex

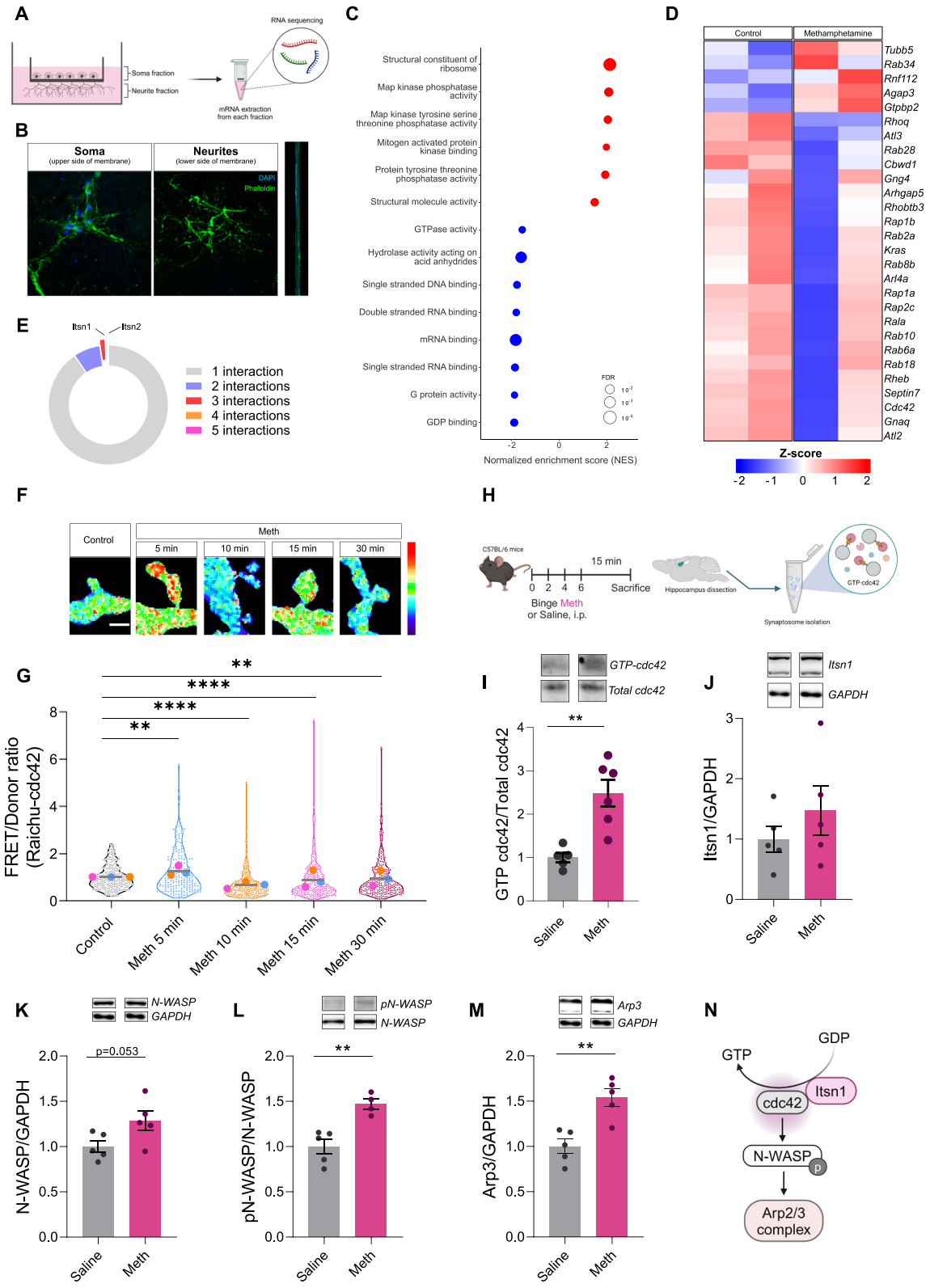

activity and a down-regulation of GTPase activity, GDP binding, single stranded DNA binding and single and double stranded RNA binding. Given the pronounced alterations in Rho GTPase-related signaling and their critical role on regulation of cell morphology changes, the genes involved in the "GTPase cycle" ontology term found in neurites were identified and their relative expression value (z-score of each gene across sample) was plotted in a heatmap (Fig. 3D). To

validate this analysis, we selected one of the proteins identified in this heatmap and confirmed its functional relevance for Meth induced changes in neuronal ramification (Suppl. Figure 3A-E). To uncover potential common signaling pathways regulating GTPase cycle, we plotted a protein–protein interaction network focusing on the first shell of interactors (first 10) of each gene within the GTPase cycle ontology term (Suppl. Table 3A). Most terms exhibited limited connectivity (with 1 or 2 direct interactions), while a subset of genes emerged as highly connected regulatory nodes. Among these, Intersectin (Itsn) 1 and 2 displayed the highest degree of connectivity, establishing 4 and 5 direct interactions, respectively (Fig. 3E). The identification of Itsn1/2 as central molecular scaffolds within Meth-altered Rho GTPase networks suggests that these proteins may serve as key regulators of neurite-specific cytoskeletal signaling.

An identical analysis in the soma fraction was conducted showing that Meth exposure did not induce the same transcriptional shift as in neurites. Instead, the genes involved in the "GTPase cycle" ontology term displayed an enrichment of microtubule-associated regulatory pathways. The microtubule associated protein tau (MAPT), emerged as the most highly connected node, establishing a maximum of 4 interactions, while 8 proteins exhibited 3 interactions, mostly related to tubulin-alpha subunits (Suppl. Figure 4A and B, Suppl. Table 3B).

These data highlight a distinct compartmentalization of Meth's effects on hippocampal neurons. While neurites display broad dysregulation of Rho GTPase pathways, the soma primarily shifts to microtubule-associated regulation, suggesting that Meth targets distinct cytoskeletal elements depending on subcellular localization. Importantly, these findings demonstrate the necessity of neurite-soma separation, as bulk RNA-seq would have failed to detect these spatially restricted molecular disruptions.

The established function of Itsn1 as a guanine exchange factor (GEF) for cdc42 [40] raises the possibility that Meth-induced dysregulation of Rho GTPase signaling is mediated through a cdc42 signaling axis, driving structural remodeling and spine reorganization in neurites. Cdc42 is a critical orchestrator of synaptic function, and both pre- and post-synaptic activity, thereby playing a pivotal role in synaptic remodeling and long-term plasticity [17, 41]. It has been demonstrated that in dendritic spines undergoing structural plasticity, cdc42 quickly becomes activated, followed by a 5 min decay and a phase of persistent activation [42]. Furthermore, cdc42 activation remained restricted to the stimulated spine [42], where it serves as a precursor for sustained synaptic modifications. Of note, the quick "on and off" nature of RhoGTPases activity justifies the temporal differences observed soon after Meth exposure, when compared to the 24 h timepoint (RNASeq).

Cdc42 activity is required to stabilize spine structure and function [43], therefore we hypothesized that Meth-induced cytoskeletal alterations may be driven by an aberrant modulation of cdc42 signaling. Primary hippocampal neurons were transfected with the Raichu-cdc42 FRET probe [44], a biosensor that enables live-cell imaging of cdc42 activity with high spatiotemporal resolution. This approach allowed us to visualize dynamic changes in cdc42 activation in single dendritic spines, providing insights into the temporal sequence of Meth-induced signaling events. Upon acute Meth stimulation (100 µM), we observed a rapid and transient increase in cdc42 activity, peaking at 5 min post-stimulus (Fig. 3F and G), consistent with an immediate cytoskeletal response to Meth. However, rather than stabilizing at baseline levels, cdc42 activity decreased from 10 min onward, ultimately falling below baseline levels post-stimulus (Fig. 3F and G). This biphasic activation-suppression pattern suggests that Meth initially induces an acute burst of cdc42 signaling, likely triggering rapid actin remodeling within dendritic spines. However, this activation is not sustained, and the subsequent suppression of cdc42 below baseline levels may impair the structural reinforcement necessary for long-term spine stability.

To validate our findings in vivo, we exposed WT mice to binge administration of Meth, as before, and isolated hippocampal synaptoneurosomes 15 min following the last administration (Fig. 3H), to evaluate cdc42 activity providing a direct in vivo biochemical validation. Consistent with our in vitro results, Meth administration significantly increased the ratio of cdc42-GTP to total cdc42, confirming that Meth activates cdc42 within synaptic compartments (Fig. 3I). This further supports the notion that Meth-induced cdc42 activation is spatially restricted to synaptic regions, likely occurring within dendritic spines.

Itsn1 was shown to be involved, through cdc42, in actin polymerization and dendritic spine morphogenesis [20, 21, 45, 46], and in long-term memory and LTP in the hippocampus [47]. We performed a RT-qPCR and found increased expression levels of Itsn1 mRNA expression in Meth-exposed hippocampal cultures when compared to PBS-exposed cultures (Suppl. Figure 4C) (this was not apparent in the previous RNASeq results, likely due to the lower number of experimental replicates and different sample preparations). No differences were found in Itsn2 mRNA expression in Meth-exposed neurons (Suppl. Figure 4D). To validate the role of Itsn1 signaling in the regulation of cdc42 after Meth exposure, in synaptoneurosomes also collected 15 min following the binge protocol, we assessed the expression of Itsn1, N-WASP, pN-WASP and Arp3 (Fig. 3J-N) showing Meth-induced increases in N-WASP ($p = 0.052$), pN-WASP and Arp3. At this timepoint, however, Itsn1 expression did not reach a significant increase.

The Arp3 subunit of Arp2/3 complex has been previously linked to dendritic spine development and synapse formation in hippocampal neurons [48]. Interestingly, in vitro we found an increase of Arp3 in synaptoneurosomes (Suppl. Figure 4E) of primary hippocampal neurons exposed to Meth (100 µM) for 15 min, which likely further promotes an elevated Arp2/3 complex activity downstream of cdc42 activation and its interaction with N-WASP [40].

The localized activation of Itsn1/cdc42 axis in synaptic compartments aligns with the idea that Meth preferentially targets actin regulatory pathways in neurites rather than inducing global changes in Rho GTPase activity throughout the neuron. However, the biphasic nature of cdc42 activation in vitro suggests that Meth's effects on spine plasticity may not be sustained, potentially leading to long-term destabilization of synaptic contacts. Together, these findings establish cdc42 as a relevant molecular target of Meth-induced signaling alterations, positioning it as a central mediator of Meth-driven structural remodeling in neurites.

Cdc42 inhibition prevented Meth-induced neuronal remodeling in vitro

Given cdc42's pivotal role in dendritic spine morphogenesis, actin cytoskeletal organization, and synaptic plasticity, we sought to determine whether Meth-induced structural changes depend on cdc42 activation. To achieve this, we disrupted cdc42 signaling using both pharmacological and genetic approaches to assess whether blocking cdc42 activity is sufficient to prevent Meth-induced neuronal remodeling.

Importantly, to establish that Itsn1 is required for Meth-induced neuronal remodeling, we transfected primary hippocampal neurons with a miRNA that targets Itsn1, previously shown to disrupt dendritic spine maturation during development [20] (Fig. 4A). Using this approach, GFP^{+} neurons show a decrease of Itsn1 expression, as expected (Suppl. Figure 5A). These neurons were then exposed to Meth or PBS (Control) for 24 h. We found that in neurons expressing miRNA Itsn1, Meth was unable to increase neurite length (Fig. 4B) or ramification (Fig. 4C, GFP transfected neurons were used as control). Importantly, dendritic spine density remained unaltered (Fig. 4D–I) across all types of dendritic spines in neurons expressing miRNA Itsn1. In control groups (GFP transfected cultures), an overall Meth-induced increase in dendritic spine density was observed, as expected.

To pharmacologically inhibit cdc42 activation, we used Zcl278, a selective inhibitor that prevents the interaction between Itsn1 and cdc42, thereby blocking Itsn1-mediated activation of cdc42 [49]. Primary hippocampal neurons were transfected with GFP and treated with 50 µM Zcl278 for 30 min before Meth exposure (100 µM Meth, 24h) (Suppl. Figure 5B). Neurons pretreated with Zcl278 did not display Meth-induced neurite elongation, as total neurite length remained at control levels (Suppl. Figure 5C). Similarly, Meth-induced increases in dendritic ramification were abolished, as shown by Sholl analysis (Suppl. Figure 5D), confirming that cdc42 activation is essential for Meth-driven cytoskeletal complexity.

At the synaptic level, Zcl278 inhibition of cdc42 prevented Meth-induced increases in dendritic spine density (Suppl. Figure 5E and F) across all major spine categories, including filopodia (Suppl. Figure 5G), thin spines (Suppl. Figure 5H), stubby spines (Suppl. Figure 5I), and mushroom spines (Suppl. Figure 5J). This suggests that cdc42 activation is essential for both structural synapse formation and synaptic remodeling under Meth exposure.

To further confirm that cdc42 is necessary for Meth-induced neuronal remodeling, we used a genetic approach, to transfect cultured primary hippocampal neurons with a dominant negative form of cdc42 (cdc42 DN), that prevents endogenous cdc42 activation. As observed with Zcl278 pretreatment, neurons expressing cdc42 DN failed to exhibit Meth-induced structural remodeling. Total neurite length remained unchanged (Fig. 4J and K), as did ramification (Fig. 4L). Dendritic spine density remained at control levels (Fig. 4M-R), confirming that cdc42 activation is required for Meth-induced alterations. Together, these results establish that Meth-induced neuronal remodeling importantly depend on cdc42 activity.

Binge meth administration drives structural and functional plasticity in the hippocampus via cdc42

While our *in vitro* findings strongly suggested cdc42 is crucial for Meth-induced remodeling, we aimed at validating these results *in vivo* using a conditional knockout approach. By selectively depleting cdc42 in hippocampal neurons, we sought to determine whether the absence of cdc42 would inhibit Meth-induced structural synaptic changes elicited by binge Meth administration.

To achieve this goal, $cdc42^{fl/fl}$ mice were intravenously injected with AAV-PHP.eB encoding tdTomato, allowing sparse labeling of hippocampal neurons (Fig. 5A). One week later, the mice underwent stereotaxic injection of AAVs expressing GFP (control) or Cre-GFP, under the regulation of the synapsin promoter, to ensure selective ablation of cdc42 floxed alleles in hippocampal neurons (Fig. 5B). Twenty-eight days after surgery, mice were subjected to a binge administration of Meth (4 × 5 mg/kg, i.p., every 2 h) and the morphology of CA1 pyramidal neurons was analyzed 24 h after the first Meth injection (Fig. 5C). Using this strategy, we confirmed an efficient depletion of cdc42 in the hippocampus (Fig. 5D).

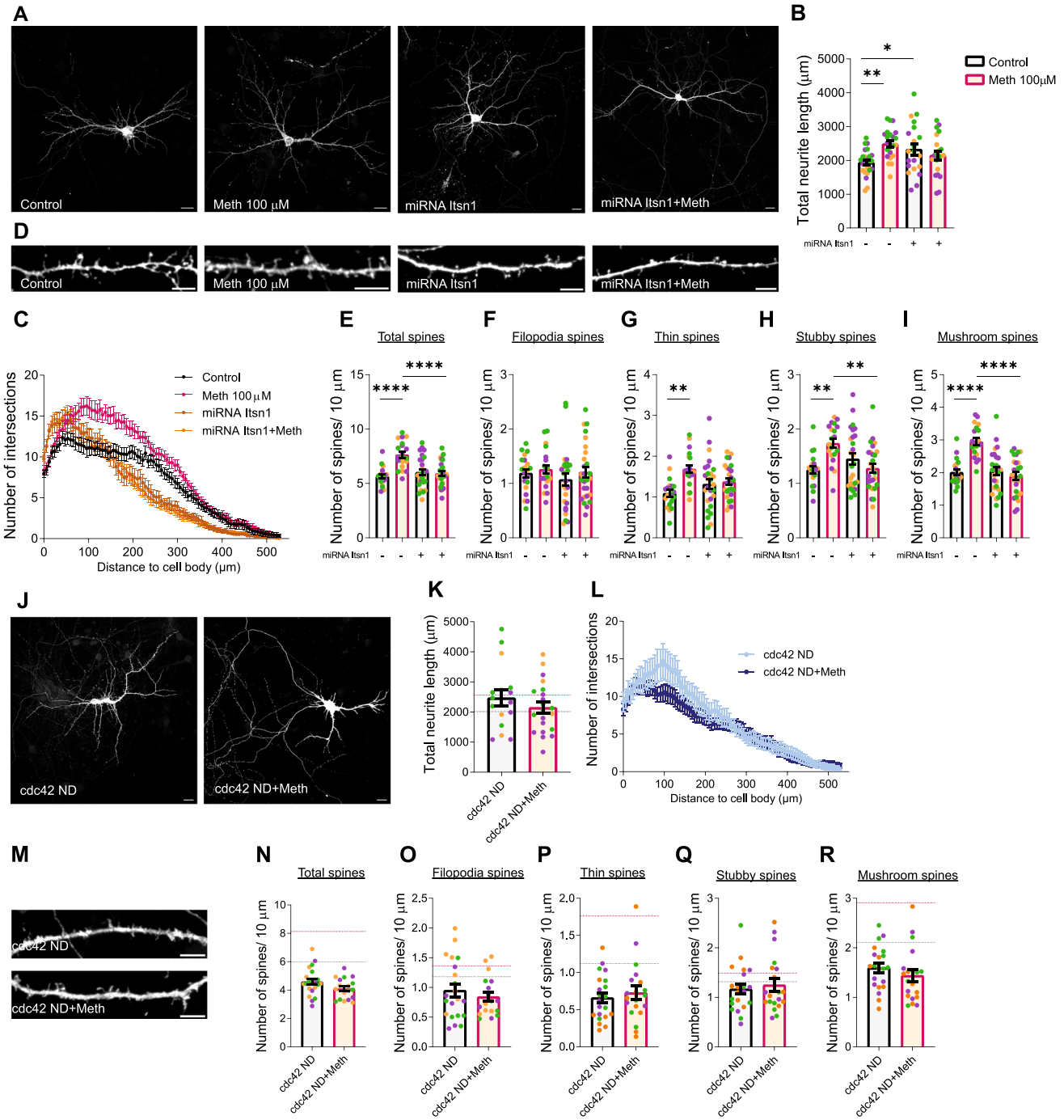

In control mice (cdc42$^{fl/fl}$; hSyn-GFP), as expected, Meth administration resulted in substantial structural remodeling. Neurons exhibited increased total neurite length, confirming Meth-induced neuronal outgrowth in the CA1 region (Fig. 5E). Sholl analysis revealed enhanced dendritic ramification, further supporting the role of Meth in driving cytoskeletal complexity (Fig. 5F). Morphological reconstructions of CA1 pyramidal neurons illustrate these Meth-driven structural changes (Fig. 5G). At the synaptic level, Meth-treated control mice exhibited increased dendritic spine density, indicative of enhanced excitatory connectivity (Fig. 5H and I). Mushroom spine density was significantly elevated, suggesting that Meth increases the number of structurally mature, functionally stable synapses (Fig. 5J-M). Remarkably, in the absence of cdc42, these Meth-induced morphological changes were abolished. In cdc42$^{fl/fl}$; hSyn-Cre-GFP mice, Meth administration failed to induce neurite elongation, dendritic branching, or increases in dendritic spine density (Fig. 5E-I). The absence of Meth-induced mushroom spine formation (Fig. 5J) further

Fig. 4 Cdc42 inhibition prevented Meth-induced neuronal remodeling in vitro. **A**: Representative images of primary hippocampal neurons transfected with GFP (Control) or miRNA targeting Itsn1, that expresses EmGFP as a reporter, and treated with PBS (Control) or 100 µM Meth treatment for 24h (scale bar: 20 µm). Graphs display (mean ± SEM) **B**: total neurite length *$p<0.05$ **$p<0.01$ (linear mixed analysis with the culture fitted as random effect followed by a Tukey–Kramer correction) and **C**: ramification (sholl) analysis (n = 21–24 neurons from 3 independent cultures) (two-way ANOVA revealing a significant effect for the distance to the cell body ($p<0.0001$), treatment ($p<0.0001$), and interaction between factors ($p<0.0001$)). **D**: Representative images of neurons transfected with GFP (Control) or miRNA targeting Itsn1 and treated with PBS (Control) or 100 µM Meth treatment for 24h (scale bar: 5 µm). Graphs display (mean ± SEM) **E**: total dendritic spine density, **F**: filopodia spine density, **G**: thin spine density, **H**: stubby spine density and **I**: mushroom spine density **$p<0.01$ ****$p<0.0001$ (linear mixed analysis with the culture fitted as random effect followed by a Tukey–Kramer correction revealing no significant differences) (n = 20–27 dendrite segments from 3 independent cultures). **J**: Representative images of primary hippocampal neurons transfected with cdc42 DN and treated with PBS (Control) or 100 µM Meth treatment for 24h (scale bar: 20 µm). Graphs display (mean ± SEM) **K**: total neurite length (linear mixed analysis with the culture fitted as random effect followed by a Tukey–Kramer correction revealing no significant differences) and **L**: ramification (sholl) analysis (n = 17–21 neurons from 3 independent cultures) (two-way ANOVA revealing significant effects for treatment ($p<0.0001$) and distance to cell body ($p<0.0001$), but no interaction between factors). **M**: Representative images of primary hippocampal neurons transfected with cdc42 DN and treated with PBS (Control) or 100 µM Meth treatment for 24h (scale bar: 5 µm). Graphs display (mean ± SEM) N: total dendritic spine density, **O**: filopodia spine density, **P**: thin spine density, **Q**: stubby spine density and **R**: mushroom spine density (linear mixed analysis with the culture fitted as random effect followed by a Tukey–Kramer correction revealing no significant differences) (n = 18–21 dendrite segments from 3 independent cultures). Dash lines represent: Control (grey) and 100 µM Meth (pink) values from Fig. 2. Each circle represents a hippocampal neuron/dendrite segment and different colors represent different independent cultures

supports the notion that cdc42 activation is necessary for Meth-driven structural plasticity in the hippocampus.

Finally, we recorded synaptic responses in hippocampal slices from $cdc42^{fl/fl}$; hSyn-GFP or $cdc42^{fl/fl}$; hSyn-Cre-GFP mice receiving binge Meth, 24 h after the first administration. As before, low-frequency stimulation of Schaffer collateral afferents induced a transient form of LTD (Fig. 5N). As expected, the increase in fEPSP slope was higher ($p = 0.06$) at T2 in Meth-administered $cdc42^{fl/fl}$; hSyn-GFP mice, compared with saline injected controls. This effect was prevented in the absence of cdc42 (Meth-administered $cdc42^{fl/fl}$; hSyn-Cre-GFP mice) (Fig. 5O), confirming that cdc42 activation is crucial for Meth-induced increases in synaptic plasticity. The impaired maintenance of LTP Meth administration in control mice ($cdc42^{fl/fl}$; hSyn-GFP) was prevented in the absence of cdc42 (Suppl. Figure 6A and B). Interestingly, although LTP levels are much higher in $cdc42^{fl/fl}$; hSyn-Cre-GFP Meth-treated animals, the LTP decay is lower than in $cdc42^{fl/fl}$; hSyn-GFP Meth-treated animals. This shows that comparing LTP levels between conditions can be misleading when not considering the temporal evolution of synaptic enhancement.

These data provide direct in vivo evidence that cdc42 is an essential mediator of Meth-induced neuronal remodeling and synaptic activity. The fact that selective depletion of cdc42 prevented Meth-induced remodeling and altered synaptic activity, underscores its critical role in orchestrating cytoskeletal and synaptic maladaptations in response to binge Meth exposure.

Discussion

In the present study, we explored the signaling mediating Meth-induced changes in hippocampal neurons' cytoarchitecture, highlighting Itsn/cdc42 as critical regulators. Using embryonic primary hippocampal cultures, we were able to recapitulate psychostimulant-induced neuronal remodeling, with an increase in neurite length, ramification and dendritic spine density, which allowed a compartmentalized analysis of Meth-induced changes separately in neurites and soma.

Using this approach, we demonstrated that subcellular localization is a key factor in determining the signaling pathways regulating Meth effects. Through an RNASeq approach, we identified Itsn1 and cdc42 as critical regulators of Meth-induced neuronal remodeling.

Our findings are aligned with recent studies on the role of cdc42 in psychostimulant-induced neuronal plasticity. Tu and colleagues demonstrated that cdc42 signaling in the nucleus accumbens mediated Meth-induced increase in total dendritic length, ramifications and dendritic spines and regulated Meth-induced conditioned place preference [10]. Other authors reported transient increases in GTP-bound cdc42 in the hippocampus following several days of cocaine [16] or Meth [11]. In the present work, we show that acute exposure to Meth is sufficient to rapidly (15 min) increase GTP-bound cdc42 in the hippocampus, importantly adding Itsn1 as a key regulator of cdc42 activation upon Meth administration. Itsn interacts with cdc42 to induce actin assembly via N-WASP and Arp2/3 complex [45] and has also been shown to be involved in dendritic spine morphogenesis [20]. In line with this, we found an increase in pN-WASP and Arp3 expression in hippocampal synaptosomes of mice exposed to a binge administration of Meth. Interestingly, two phosphorylation sites have been reported in Itsn1 that could regulate its function [50], since posttranslational modifications are common mechanisms for modulation of several Rho GEFs [12]. Under Meth, Itsn1 modulation may occur via activation of group I mGlu receptors [50], which

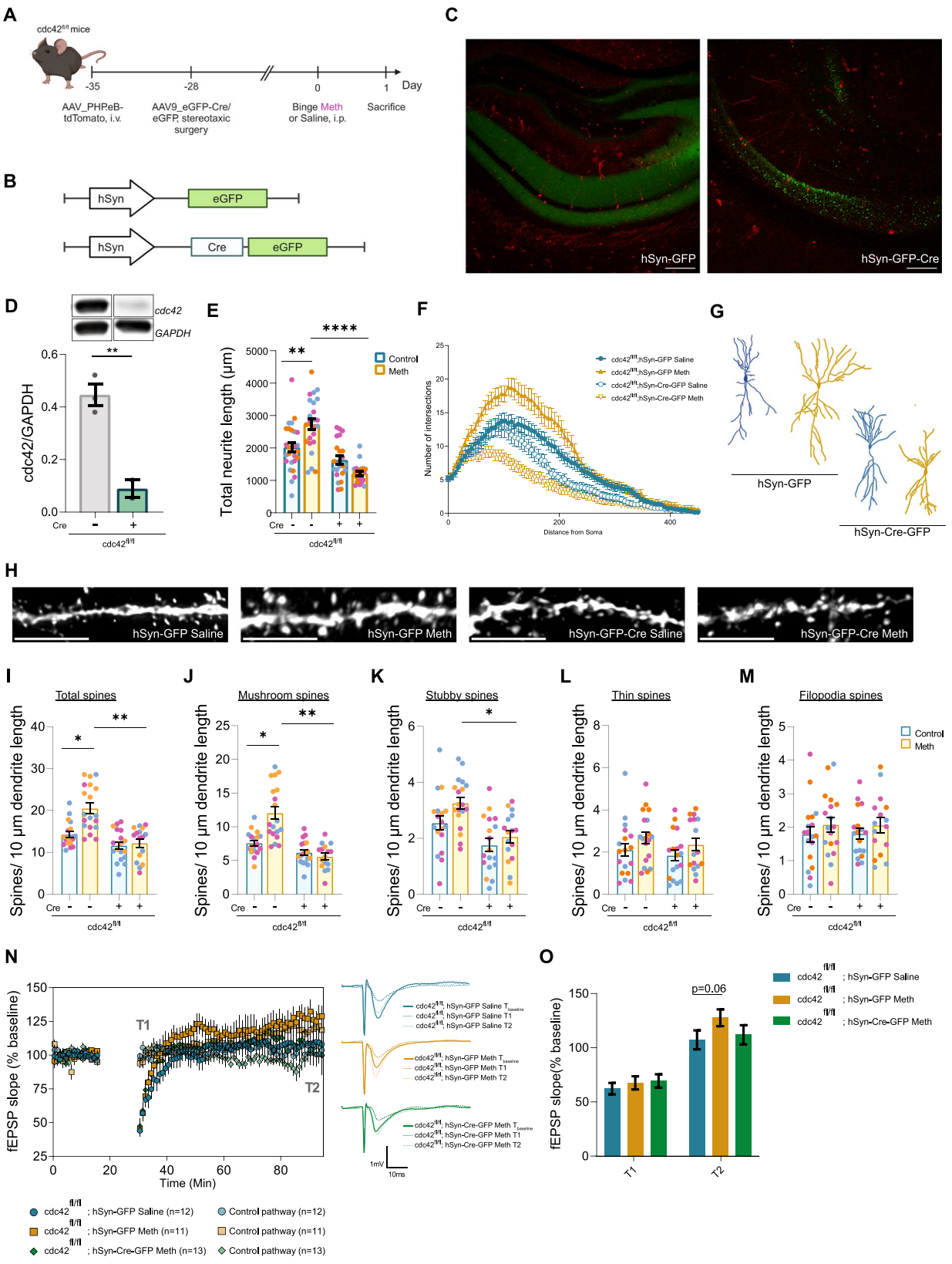
A
cdc42fl/fl mice
-35
-28
0
1
Day
AAV_PHPeB-tdTomato, i.v.
AAV9_eGFP-Cre/eGFP, stereotaxic surgery
Binge Meth or Saline, i.p.
Sacrifice
B
hSyn
eGFP
hSyn
Cre
eGFP
C
hSyn-GFP
hSyn-GFP-Cre
D
cdc42
GAPDH
cdc42/GAPDH
Cre
cdc42fl/fl
E
Total neurite length (µm)
Control
Meth
Cre
cdc42fl/fl
F
Number of intersections
Distance from Soma
cdc42fl/fl;hSyn-GFP Saline
cdc42fl/fl;hSyn-GFP Meth
cdc42fl/fl;hSyn-Cre-GFP Saline
cdc42fl/fl;hSyn-Cre-GFP Meth
G
hSyn-GFP
hSyn-Cre-GFP
H
hSyn-GFP Saline
hSyn-GFP Meth
hSyn-GFP-Cre Saline
hSyn-GFP-Cre Meth
I
Total spines
Spines/ 10 µm dendrite length
J
Mushroom spines
K
Stubby spines
L
Thin spines
M
Filopodia spines
Control
Meth
N
fEPSP slope (% baseline)
T1
T2
Time (Min)
cdc42fl/fl; hSyn-GFP Saline T baseline
cdc42fl/fl; hSyn-GFP Saline T1
cdc42fl/fl; hSyn-GFP Saline T2
cdc42fl/fl; hSyn-GFP Meth T baseline
cdc42fl/fl; hSyn-GFP Meth T1
cdc42fl/fl; hSyn-GFP Meth T2
cdc42fl/fl; hSyn-Cre-GFP Meth T baseline
cdc42fl/fl; hSyn-Cre-GFP Meth T1
cdc42fl/fl; hSyn-Cre-GFP Meth T2
1mV
10ms
cdc42fl/fl; hSyn-GFP Saline (n=12)
cdc42fl/fl; hSyn-GFP Meth (n=11)
cdc42fl/fl; hSyn-Cre-GFP Meth (n=13)
Control pathway (n=12)
Control pathway (n=11)
Control pathway (n=13)
O
fEPSP slope(% baseline)
p=0.06
T1
T2
cdc42fl/fl; hSyn-GFP Saline
cdc42fl/fl; hSyn-GFP Meth
cdc42fl/fl; hSyn-Cre-GFP Meth

Fig. 5 Binge Meth Administration Drives Structural and Functional Plasticity in the Hippocampus via cdc42. **A**: Schematic representation of experimental timeline. Adult male cdc42$^{fl/fl}$ mice were intravenously injected with an AAV_PHP.eB for tdTomato transduction in the CNS. One week later, mice received a stereotactic surgery for injection of hSyn-GFP or hSyn-Cre-GFP in the hippocampus. Twenty-eight days later, mice received a binge administration of 5 mg/kg Meth, i.p. four times, with two-hours interval between each injection or saline (control). Twenty-four hours after the first administration, mice were sacrificed and the morphology of neurons in the CA1 region of the hippocampus analyzed. **B**: Schematic representation of stereotaxically injected AAVs. **C**: Representative images of hippocampal infection (scale bar: 200 µm) (green: GTP, red: tdTomato). Graph display (mean ± SEM) **D**: cdc42 levels normalized to GAPDH $p^{**} < 0.001$ (unpaired t-test) (n = 2–3 mice/group). Graphs display (mean ± SEM) **E**: total neurite length of neurons of the CA1 region $^{**}p < 0.01$ $^{****}p < 0.0001$ (linear mixed analysis with the animal fitted as a random effect model followed by a Tukey–Kramer correction) and **F**: ramification (sholl) analysis $^{****}p < 0.0001$ (two-way ANOVA revealing significant effects for treatment ($p < 0.0001$) and distance to cell body ($p < 0.0001$), with interaction between factors ($p < 0.0001$) (n = 5–11 neurons/animal from 3 mice per group). **G**: Representative tracings of CA1 neurons. **H**: Representative images of dendritic spines (scale bar: 5 µm). Graphs display (mean ± SEM) **I**: total dendritic spine density, **J**: mushroom spine density, **K**: stubby spine density, **L**: thin spine density and **M**: filopodia spine density $^{*}p < 0.05$ $^{**}p < 0.01$ (linear mixed analysis with the animal fitted as a random effect followed by a Tukey–Kramer correction). Each circle represents each hippocampal neuron/dendrite segment and each color represents each mice. **N**: Summary plot of normalized fEPSP slope measurements recorded in the CA1 region of the hippocampus (mean ± SEM) of cdc42$^{fl/fl}$; hSyn-GFP saline (blue round symbols), cdc42$^{fl/fl}$; hSyn-GFP Meth (yellow square symbols) or cdc42.$^{fl/fl}$; hSyn-Cre-GFP Meth (green diamond symbols) treated mice after LTD induction with a low frequency burst stimulation. Slice viability was assessed by recording a second independent pathway that did not show a significant decrease throughout the recording. Right: average fEPSPs at baseline (solid line), T1 (dashed line) and T2 (dotted line). Scale bar: 1 mv, 10 ms. **O**: Summary plot showing the percentage of LTD decay for the time window at T1 and T2 (two-way ANOVA with two-stage step-up method of Benjamini, Krieger and Yekutiel for multiple comparisons revealing no significant differences) (n = 11–12 slices from 4–5 mice per group)

are involved in Meth-induced reinforcement and seeking behavior [51], and maintenance of Meth-induced conditioned place preference [52].

Recently, we have shown that Meth induces a rapid increase in astrocytic cdc42 activity, which was linked to intracellular calcium dynamics and glutamate release [24]. Previous studies identified cdc42 as an important regulator of long-term maintenance of structural spine plasticity during the sustained phase of spine enlargement [53], and its activation was shown to be restricted to stimulated spine heads [43]. Interestingly, mature spines are more likely to compartmentalize calcium action within the spine head than thin spines. This process is controlled by spine neck dimensions, and allows for the modulation of signaling cascades that strengthen or weaken spine synapses [37]. The actin cytoskeleton and its regulatory proteins have been proposed to be key in stabilizing spine structure and maintaining long-term memory [34]. Supporting that, maintenance of Meth-induced conditioned place preference has been impaired through actin-cycling inhibition [54]. Given their roles, cdc42 and Itsn1 are likely relevant players at inducing and stabilizing Meth-associated memories and impairing synaptic homeostasis.

Our comparison between in vitro and in vivo effects of Meth demonstrates similar morphological results—increased neurite length and ramification, dendritic spine density and maturation, decreased dendritic head, and no alterations on PSD95/VGLUT1 colocalization. However, in vitro, Meth decreased spontaneous firing, while in vivo we observed increased synaptic transmission. Likewise, it has also been demonstrated that repeated Meth exposure increases baseline synaptic transmission and decreases LTP in the CA1 region of the hippocampus [4]. This effect was found to be modulated by activation of dopamine and serotonin receptor systems in the hippocampus. On the other hand, and in agreement with our in vitro results, it was reported [55], in rat primary cultured hippocampal cultures, a decrease in spontaneous excitatory postsynaptic currents after exposure to 100 µM, and this effect was not dependent on the dopaminergic system. Additionally, our results indicate that low-frequency stimulation of Schaffer collateral afferents induce short term depression in control mice followed by a return to baseline levels, but in Meth-treated mice, it led to a transient form of LTP. This LTD-to-LTP conversion has been previously observed by Larsen and colleagues [56], that described how β-adrenergic stimulation enabled increased surface expression of GluA1, a feature of LTP occurring in response to a LTD stimulus. This effect was regulated via NMDAR-mediated non-ionotropic scaffolding of CaMKII targeting of excitatory synapses [56]. Itsn1 has a critical role in internalization of the AMPAR subunit GluA1 in dendritic spines [50] and has also been shown to associate with NMDAR and PSD95, likely acting as a scaffold protein that stabilizes NMDAR at the post-synapse [23], raising the question of whether altered levels of Itsn1 are causing aberrant receptor signaling in response to Meth. AMPAR-silent synapses have been extensively demonstrated after psychostimulant administration, and represent a small population of neuronal substrates encoding for drug-associated memories [57]. Recruitment of calcium-permeable AMPARs takes place during withdrawal [58], was found to occur more rapidly in Meth-treated rats (in the nucleus accumbens core), and seems to increase GluA1 translation during Meth craving [59]. Nonetheless, it has also been suggested that a serotoninergic mechanism may be responsible for increases in baseline transmission, due to serotoninergic potentiation of excitatory synaptic transmission [55]. Overall, our results indicate that Meth administration leads to an increase in synaptic transmission, and the

higher level of LTP suggests an increase in neuronal excitability, but further studies are needed to test this hypothesis.

On the other hand, we did not find increased PSD95 expression neither in Meth-treated animals nor in primary hippocampal neurons exposed to Meth. This suggests that the spines newly formed are likely transient and unstable, since spines lacking this scaffolding protein are highly dynamic [60]. Changes in the expression of synaptic proteins upon psychostimulant exposure were also reported, including downregulation of PSD95 in the striatum during cocaine withdrawal [61], while during the self-administration period, there is evidence of an upregulation of PSD95 in the cortex [62]. Our results suggest that rather than enhancing network excitability, Meth appears to disrupt the stability of hippocampal circuits, leading to reduced synaptic output, potentially compromising information processing. This aligns with our in vivo findings, where Meth altered responses to LTP and LTD stimuli, highlighting its profound impact on synaptic homeostasis. Importantly, we demonstrate that neuronal cdc42 depletion in the hippocampus prevents Meth-induced remodeling and synaptic transmission. A major limitation of this study is that only male mice were used, which may limit the generalization of our findings, since it is known that biological sex discrepancies are present in various stages of drug addiction [63].

The present results suggest a process of synaptic reorganization, supporting the hypothesis of a Itsn1/cdc42 role in the formation of drug-related maladaptive memories. Addiction is often characterized as a hijacking of memory and learning mechanisms by maladaptive responses, recruited to foster drug-seeking and drug-taking. These actions are associated to specific contexts and cues, that become precipitators of relapse and promote drug-seeking behavior [64].

In summary, the present results, highlight relevant compartment-associated differences in the activity of the Itsn1/cdc42 pathway that critically regulates Meth action at the neuronal level, particularly in dendritic spines. Our results also reinforce the role of cdc42 activation on LTP maintenance and structural plasticity, further emphasizing its relevance in the context of drug use. Unveiling how Rho GTPases and their regulators are spatiotemporally modulated by psychoactive substances in neurons and glial cells will uncover novel therapeutic targets and interventions in substance use disorders.

Supplementary Information The online version contains supplementary material available at https://doi.org/10.1007/s00018-025-05890-8.

Acknowledgements We acknowledge the invaluable role of FCT—Fundação para a Ciência e a Tecnologia, I.P. in supporting fundamental research. We acknowledge the support of the following i3S Scientific Platforms: Advanced Light Microscopy (ALM), a member of the national infrastructure PPBI-Portuguese Platform of BioImaging (supported by POCI-01-0145-FEDER-022122), and Animal Facility, and we thank Maria Azevedo, Mafalda Sousa and Sofia Lamas from these facilities for their technical support. We also thank Andreia Garcia and Sara Rodrigues for their contribution to this manuscript. We thank the High-Throughput Genomics Group at the Wellcome Trust Centre for Human Genetics (funded by Wellcome Trust grant reference 090532/Z/09/Z) and the Bioinformatics Group of the Babraham Institute for the generation of Sequencing data.

Author contributions Conceptualization: Ana Filipa Terceiro, Andrea Lobo, Renato Socodato, João B. Relvas, Rosalina Fonseca, Teresa Summavielle; Methodology: Ana Filipa Terceiro, Andrea Lobo, Teresa Canedo, Ana Isabel Silva, Miguel Aroso, Gabriela M. Morello, Paulo Aguiar, Ana Luísa Carvalho, Teresa Summavielle; Formal analysis and investigation: Ana Filipa Terceiro, Andrea Lobo, Teresa Canedo, Ana Isabel Silva, Bruno Cavadas, Lia Carvalhais, Miguel Aroso, Ana Magalhães, Rosalina Fonseca, Teresa Summavielle; Writing—original draft preparation: Ana Filipa Terceiro, Andrea Lobo, Teresa Summavielle; Writing—review and editing: All authors; Funding acquisition: Teresa Summavielle; Resources: Bruno Cavadas, Paulo Aguiar, Ana Luísa Carvalho, Rosalina Fonseca, João Relvas; Supervision: Teresa Summavielle.

Funding This work was funded by National Funds through FCT—Fundação para a Ciência e a Tecnologia, I.P., under the project PTDC/SAU-TOX/0067/2021 (in Summavielle's lab), this project has also supported the work of TC. This work is also a result of the project NORTE2030-FEDER-01711200 - ERA Chair NCbio_2030 , supported by Norte Portugal Regional Operational Programme (NORTE 2030), under the PORTUGAL 2030 Partnership Agreement, through the European Regional Development Fund (FEDER)". AIS and AFT were supported by FCT fellowships (SFRH/BD/144324/2019, 2020.07188.BD). RS helde employment contracts financed by national funds through FCT –in the context of the program-contract described in paragraphs 4, 5, and 6 of art. 23 of Law no. 57/ 2016, of August 29, as amended by Law no. 57/2017 of July 2019 and a FCT 023.06380. CEECIND. TS, BC and RF are funded by FCT through 2022.03699. CEECIND CEECINST/00123/2021 and CEECINST.2802.2022, respectively.

Data availability The authors confirm that the data supporting the findings of this study are available within the article and its Supplementary material.

Declarations

Ethics approval All mice experiments were in compliance with the Directive 2010/63/EU and approved by Direcção Geral de Alimentação e Veterinária (DGAV) and i3S Animal Ethical Committee (ref.2018–13-TS and DGAV ref.003891/2019–02-15). Researchers involved in animal experimentation were FELASA certified. All efforts were made to minimize animal suffering and the number of animals used.

Competing interests The authors have no relevant financial or non-financial interests to disclose.

References

1. Pandey S, Miller CA (2024) Targeting the cytoskeleton as a therapeutic approach to substance use disorders. Pharmacol Res 202:107143. https://doi.org/10.1016/j.phrs.2024.107143
2. Kutlu MG, Gould TJ (2016) Effects of drugs of abuse on hippocampal plasticity and hippocampus-dependent learning and memory: contributions to development and maintenance of addiction. Learn Mem 23:515–533. https://doi.org/10.1101/lm.042192
3. North A, Swant J, Salvatore MF, Gamble-George J, Prins P, Butler B, Mittal MK, Heltsley R, Khoshbouei H et al (2013) Chronic methamphetamine exposure produces a delayed, long-lasting memory deficit. Synapse 67:245–257. https://doi.org/10.1002/syn.21635
4. Swant J, Chirwa S, Stanwood G, Khoshbouei H (2010) Methamphetamine reduces LTP and increases baseline synaptic transmission in the CA1 region of mouse hippocampus. PLoS ONE 5:e11382. https://doi.org/10.1371/journal.pone.0011382
5. Bisagno V, Ferguson D, Luine VN (2002) Short toxic methamphetamine schedule impairs object recognition task in male rats. Brain Res 940:95–101
6. Klambatsen A, Nygard SK, Chang AJ, Quinones V, Jenab S (2019) Sex differences in memory and intracellular signaling after methamphetamine binge treatment. Brain Res 1711:16–22. https://doi.org/10.1016/j.brainres.2019.01.010
7. Belcher AM, O'Dell SJ, Marshall JF (2005) Impaired object recognition memory following methamphetamine, but not p-chloroamphetamine- or d-amphetamine-induced neurotoxicity. Neuropsychopharmacology 30:2026–2034. https://doi.org/10.1038/sj.npp.1300771
8. Golden SA, Russo SJ (2012) Mechanisms of psychostimulant-induced structural plasticity. Cold Spring Harb Perspect Med. https://doi.org/10.1101/cshperspect.a011957
9. Dietz DM, Sun H, Lobo MK, Cahill ME, Chadwick B, Gao V, Koo JW, Mazei-Robison MS, Nestler EJ et al (2012) Rac1 is essential in cocaine-induced structural plasticity of nucleus accumbens neurons. Nat Neurosci 15:891–896. https://doi.org/10.1038/nn.3094
10. Tu G, Ying L, Ye L, Zhao J, Liu N, Li J, Liu Y, Zhu M, Zhang L et al (2019) Dopamine D1 and D2 receptors differentially regulate Rac1 and Cdc42 signaling in the nucleus accumbens to modulate behavioral and structural plasticity after repeated methamphetamine treatment. Biol Psychiatry. https://doi.org/10.1016/j.biopsych.2019.03.966
11. Ding J, Huang J, Tang X, Shen L, Hu S, He J, Liu T, Yu Z, Huang J et al (2022) Low and high dose methamphetamine differentially regulate synaptic structural plasticity in cortex and hippocampus. Front Cell Neurosci 16:1003617. https://doi.org/10.3389/fncel.2022.1003617
12. Hodge RG, Ridley AJ (2016) Regulating rho GTPases and their regulators. Nat Rev Mol Cell Biol 17:496–510. https://doi.org/10.1038/nrm.2016.67
13. Stankiewicz TR, Linseman DA (2014) Rho family GTPases: key players in neuronal development, neuronal survival, and neurodegeneration. Front Cell Neurosci 8:314. https://doi.org/10.3389/fncel.2014.00314
14. de Beco S, Vaidziulyte K, Manzi J, Dalier F, di Federico F, Cornilleau G, Dahan M, Coppey M (2018) Optogenetic dissection of Rac1 and Cdc42 gradient shaping. Nat Commun 9:4816. https://doi.org/10.1038/s41467-018-07286-8
15. Kiraly DD, Eipper-Mains JE, Mains RE, Eipper BA (2010) Synaptic plasticity, a symphony in GEF. ACS Chem Neurosci 1:348–365. https://doi.org/10.1021/cn100012x
16. Li J, Wu Y, Xue T, He J, Zhang L, Liu Y, Zhao J, Chen Z, Zhang L et al (2023) Cdc42 signaling regulated by dopamine D2 receptor correlatively links specific brain regions of hippocampus to cocaine addiction. Biochim et Biophys Acta (BBA) 1869:166569. https://doi.org/10.1016/j.bbadis.2022.166569
17. Kim IH, Wang H, Soderling SH, Yasuda R (2014) Loss of Cdc42 leads to defects in synaptic plasticity and remote memory recall. eLife 3. https://doi.org/10.7554/eLife.02839
18. Chidambaram SB, Rathipriya AG, Bolla SR, Bhat A, Ray B, Mahalakshmi AM, Manivasagam T, Thenmozhi AJ, Sakharkar MK et al (2019) Dendritic spines: revisiting the physiological role. Prog Neuropsychopharmacol Biol Psychiatry 92:161–193. https://doi.org/10.1016/j.pnpbp.2019.01.005
19. Kim J, Lee S, Jung K, Oh WC, Kim N, Son S, Jo Y, Kwon HB, Do Heo W (2019) Intensiometric biosensors visualize the activity of multiple small GTPases in vivo. Nat Commun 10:211. https://doi.org/10.1038/s41467-018-08217-3
20. Thomas S, Ritter B, Verbich D, Sanson C, Bourbonniere L, McKinney RA, McPherson PS (2009) Intersectin regulates dendritic spine development and somatodendritic endocytosis but not synaptic vesicle recycling in hippocampal neurons. J Biol Chem 284:12410–12419. https://doi.org/10.1074/jbc.M809746200
21. Irie F, Yamaguchi Y (2002) EphB receptors regulate dendritic spine development via intersectin, Cdc42 and N-WASP. Nat Neurosci 5:1117–1118. https://doi.org/10.1038/nn964
22. Jakob B, Kochlamazashvili G, Japel M, Gauhar A, Bock HH, Maritzen T, Haucke V (2017) Intersectin 1 is a component of the Reelin pathway to regulate neuronal migration and synaptic plasticity in the hippocampus. Proc Natl Acad Sci U S A 114:5533–5538. https://doi.org/10.1073/pnas.1704447114
23. Vollweiter D, Shergill JK, Hilse A, Kochlamazashvili G, Koch SP, Mueller S, Boehm-Sturm P, Haucke V, Maritzen T (2023) Intersectin deficiency impairs cortico-striatal neurotransmission and causes obsessive-compulsive behaviors in mice. Proc Natl Acad Sci U S A 120:e2304323120. https://doi.org/10.1073/pnas.2304323120
24. Silva AI, Socodato R, Pinto C, Terceiro AF, Canedo T, Relvas JB, Saraiva M, Summavielle T (2024) IL-10 and Cdc42 modulate astrocyte-mediated microglia activation in methamphetamine-induced neuroinflammation. Glia. https://doi.org/10.1002/glia.24542
25. Good RL, Liang LP, Patel M, Radcliffe RA (2011) Mouse strain- and age-dependent effects of binge methamphetamine on dopaminergic signaling. Neurotoxicology 32:751–759. https://doi.org/10.1016/j.neuro.2011.07.005
26. Canedo T, Portugal CC, Socodato R, Almeida TO, Terceiro AF, Bravo J, Silva AI, Magalhães JD, Summavielle T et al (2021) Astrocyte-derived TNF and glutamate critically modulate microglia activation by methamphetamine. Neuropsychopharmacology. https://doi.org/10.1038/s41386-021-01139-7
27. Gomes JR, Lobo A, Nogueira R, Terceiro AF, Costelha S, Lopes IM, Magalhaes A, Summavielle T, Saraiva MJ (2020) Neuronal megalin mediates synaptic plasticity-a novel mechanism underlying intellectual disabilities in megalin gene pathologies. Brain Commun 2:fcaa135. https://doi.org/10.1093/braincomms/fcaa135
28. Fath T, Ke YD, Gunning P, Gotz J, Ittner LM (2009) Primary support cultures of hippocampal and substantia nigra neurons. Nat Protoc 4:78–85. https://doi.org/10.1038/nprot.2008.199

29. Stagi M, Fogel AI, Biederer T (2010) SynCAM 1 participates in axo-dendritic contact assembly and shapes neuronal growth cones. Proc Natl Acad Sci U S A 107:7568–7573. https://doi.org/10.1073/pnas.0911798107
30. Catarino T, Ribeiro L, Santos SD, Carvalho AL (2013) Regulation of synapse composition by protein acetylation: the role of acetylated cortactin. J Cell Sci 126:149–162. https://doi.org/10.1242/jcs.110742
31. Yoshizaki H, Ohba Y, Kurokawa K, Itoh RE, Nakamura T, Mochizuki N, Nagashima K, Matsuda M (2003) Activity of Rho-family GTPases during cell division as visualized with FRET-based probes. J Cell Biol 162:223–232. https://doi.org/10.1083/jcb.200212049
32. Shabani S, Houlton SK, Hellmuth L, Mojica E, Mootz JR, Zhu Z, Reed C, Phillips TJ (2016) A mouse model for binge-level methamphetamine use. Front Neurosci 10:493. https://doi.org/10.3389/fnins.2016.00493
33. Holtmaat A, Svoboda K (2009) Experience-dependent structural synaptic plasticity in the mammalian brain. Nat Rev Neurosci 10:647–658. https://doi.org/10.1038/nrn2699
34. Basu S, Lamprecht R (2018) The role of actin cytoskeleton in dendritic spines in the maintenance of long-term memory. Front Mol Neurosci 11:143. https://doi.org/10.3389/fnmol.2018.00143
35. McLeod F, Marzo A, Podpolny M, Galli S, Salinas P (2017) Evaluation of synapse density in hippocampal rodent brain slices. J Vis Exp. https://doi.org/10.3791/56153
36. Bravo J, Ribeiro I, Terceiro AF, Andrade EB, Portugal CC, Lopes IM, Azevedo MM, Sousa M, Summavielle T et al (2022) Neuron-microglia contact-dependent mechanisms attenuate methamphetamine-induced microglia reactivity and enhance neuronal plasticity. Cells 11 https://doi.org/10.3390/cells11030355
37. Bourne J, Harris KM (2007) Do thin spines learn to be mushroom spines that remember? Curr Opin Neurobiol 17:381–386. https://doi.org/10.1016/j.conb.2007.04.009
38. Nusser Z, Lujan R, Laube G, Roberts JDB, Molnar E, Somogyi P (1998) Cell type and pathway dependence of synaptic AMPA receptor number and variability in the hippocampus. Neuron 21:545–559. https://doi.org/10.1016/S0896-6273(00)80565-6
39. Azevedo MM, Domingues HS, Cordelieres FP, Sampaio P, Seixas AI, Relvas JB (2018) Jmy regulates oligodendrocyte differentiation via modulation of actin cytoskeleton dynamics. Glia 66:1826–1844. https://doi.org/10.1002/glia.23342
40. Herrero-Garcia E, O'Bryan JP (2017) Intersectin scaffold proteins and their role in cell signaling and endocytosis. Biochim Biophys Acta Mol Cell Res 1864:23–30. https://doi.org/10.1016/j.bbamcr.2016.10.005
41. Shen W, Wu B, Zhang Z, Dou Y, Rao ZR, Chen YR, Duan S (2006) Activity-induced rapid synaptic maturation mediated by presynaptic cdc42 signaling. Neuron 50:401–414. https://doi.org/10.1016/j.neuron.2006.03.017
42. Murakoshi H, Wang H, Yasuda R (2011) Local, persistent activation of Rho GTPases during plasticity of single dendritic spines. Nature 472:100–104. https://doi.org/10.1038/nature09823
43. Nakahata Y, Yasuda R (2018) Plasticity of spine structure: local signaling, translation and cytoskeletal reorganization. Front Synaptic Neurosci 10:29. https://doi.org/10.3389/fnsyn.2018.00029
44. Itoh RE, Kurokawa K, Ohba Y, Yoshizaki H, Mochizuki N, Matsuda M (2002) Activation of Rac and Cdc42 video imaged by fluorescent resonance energy transfer-based single-molecule probes in the membrane of living cells. Mol Cell Biol 22:6582–6591. https://doi.org/10.1128/MCB.22.18.6582-6591.2002
45. Hussain NK, Jenna S, Glogauer M, Quinn CC, Wasiak S, Guipponi M, Antonarakis SE, Kay BK, McPherson PS et al (2001) Endocytic protein intersectin-l regulates actin assembly via Cdc42 and N-WASP. Nat Cell Biol 3:927–932. https://doi.org/10.1038/ncb1001-927
46. Pechstein A, Shupliakov O, Haucke V (2010) Intersectin 1: a versatile actor in the synaptic vesicle cycle. Biochem Soc Trans 38:181–186. https://doi.org/10.1042/BST0380181
47. Malakooti N, Pritchard MA, Chen F, Yu Y, Sgambelloni C, Adlard PA, Finkelstein DI (2020) The long isoform of Intersectin-1 has a role in learning and memory. Front Behav Neurosci 14:24. https://doi.org/10.3389/fnbeh.2020.00024
48. Wegner AM, Nebhan CA, Hu L, Majumdar D, Meier KM, Weaver AM, Webb DJ (2008) N-wasp and the Arp2/3 complex are critical regulators of actin in the development of dendritic spines and synapses. J Biol Chem 283:15912–15920. https://doi.org/10.1074/jbc.M801555200
49. Friesland A, Zhao Y, Chen YH, Wang L, Zhou H, Lu Q (2013) Small molecule targeting Cdc42-intersectin interaction disrupts Golgi organization and suppresses cell motility. Proc Natl Acad Sci U S A 110:1261–1266. https://doi.org/10.1073/pnas.1116051110
50. van Gelder C, Penning R, Veth TS, Catsburg LAE, Hoogenraad CC, MacGillavry HD, Altelaar M (2020) Temporal Quantitative Proteomics of mGluR-induced Protein Translation and Phosphorylation in Neurons. Mol Cell Proteomics 19:1952–1968. https://doi.org/10.1074/mcp.RA120.002199
51. Gass JT, Osborne MP, Watson NL, Brown JL, Olive MF (2009) MGluR5 antagonism attenuates methamphetamine reinforcement and prevents reinstatement of methamphetamine-seeking behavior in rats. Neuropsychopharmacology 34:820–833. https://doi.org/10.1038/npp.2008.140
52. Herrold AA, Voigt RM, Napier TC (2013) mGluR5 is necessary for maintenance of methamphetamine-induced associative learning. Eur Neuropsychopharmacol 23:691–696. https://doi.org/10.1016/j.euroneuro.2012.05.014
53. Kim J, Lee S, Jung K, Oh WC, Kim N, Son S, Jo Y, Kwon H-B, Heo WD (2019) Intensiometric biosensors visualize the activity of multiple small GTPases in vivo. Nat Commun 10:211. https://doi.org/10.1038/s41467-018-08217-3
54. Young EJ, Aceti M, Griggs EM, Fuchs RA, Zigmond Z, Rumbaugh G, Miller CA (2014) Selective, retrieval-independent disruption of methamphetamine-associated memory by actin depolymerization. Biol Psychiatry 75:96–104. https://doi.org/10.1016/j.biopsych.2013.07.036
55. Zhang S, Jin Y, Liu X, Yang L, Ge Z, Wang H, Li J, Zheng J (2014) Methamphetamine modulates glutamatergic synaptic transmission in rat primary cultured hippocampal neurons. Brain Res 1582:1–11. https://doi.org/10.1016/j.brainres.2014.07.040
56. Larsen ME, Buonarati OR, Qian H, Hell JW, Bayer KU (2023) Stimulating beta-adrenergic receptors promotes synaptic potentiation by switching CaMKII movement from LTD to LTP mode. J Biol Chem 299:104706. https://doi.org/10.1016/j.jbc.2023.104706
57. Wright WJ, Dong Y (2021) Silent synapses in cocaine-associated memory and beyond. J Neurosci 41:9275–9285. https://doi.org/10.1523/JNEUROSCI.1559-21.2021
58. Shukla A, Beroun A, Panopoulou M, Neumann PA, Grant SG, Olive MF, Dong Y, Schluter OM (2017) Calcium-permeable AMPA receptors and silent synapses in cocaine-conditioned place preference. EMBO J 36:458–474. https://doi.org/10.15252/embj.201695465
59. Murray CH, Loweth JA, Milovanovic M, Stefanik MT, Caccamise AJ, Dolubizno H, Funke JR, Foster Olive M, Wolf ME (2019) AMPA receptor and metabotropic glutamate receptor 1 adaptations in the nucleus accumbens core during incubation of methamphetamine craving. Neuropsychopharmacology 44:1534–1541. https://doi.org/10.1038/s41386-019-0425-5
60. Berry KP, Nedivi E (2017) Spine dynamics: are they all the same? Neuron 96:43–55. https://doi.org/10.1016/j.neuron.2017.08.008

61. Wei-Dong Y, Gainetdinov RR, Arbuckle MI, Sotnikova TD, Cyr M, Beaulieu J-M, Torres GE, Grant SGN, Caron MG (2004) Identification of PSD-95 as a regulator of dopamine-mediated synaptic and behavioral plasticity. Neuron 41:625–638. https://doi.org/10.1016/s0896-6273(04)00048-0
62. McIntosh S, Howell L, Hemby SE (2013) Dopaminergic dysregulation in prefrontal cortex of rhesus monkeys following cocaine self-administration. Front Psychiatry 4:88. https://doi.org/10.3389/fpsyt.2013.00088
63. Sardari M, Mohammadpourmir F, Hosseinzadeh Sahafi O, Rezayof A (2024) Neuronal biomarkers as potential therapeutic targets for drug addiction related to sex differences in the brain: opportunities for personalized treatment approaches. Prog Neuropsychopharmacol Biol Psychiatry 134:111068. https://doi.org/10.1016/j.pnpbp.2024.111068
64. Milton AL (2023) Drug memory reconsolidation: from molecular mechanisms to the clinical context. Transl Psychiatry 13:370. https://doi.org/10.1038/s41398-023-02666-1